Article

Auxiliary Power Supply System Using Parallel-Connected DC-AC Inverter for Low-Floor Light Rail Vehicle

Paiwan Kerdtuad *, Kunjana Chaiamarit , Supat Kittiratsatcha

Posted Date: 1 May 2023

doi: 10.20944/preprints202305.0020.v1

Keywords: auxiliary power supply system; low-floor light rail vehicle; dc train; parallel-connected dc-ac inverter; variable voltage variable frequency control

Article

Auxiliary Power Supply System Using Parallel-Connected DC-AC Inverter for Low-Floor Light Rail Vehicle

Paiwan Kerdtuad [1,*], Kunjana Chaiamarit [1] and Supat Kittiratsatcha [2]

[1] Department of Electrical Engineering, Faculty of Engineering, Rajamangala University of Technology Isan, Khon Kaen Campus, Khon Kaen, Thailand; paiwan.ke@rmuti.ac.th; kunjana.ch@rmuti.ac.th

[2] Department of Electrical Engineering, School of Engineering, King Mongkut's Institute of Technology Ladkrabang, Bangkok, Thailand; supat.ki@kmitl.ac.th

* Correspondence: paiwan.ke@rmuti.ac.th; Tel.: +66 81 855 5725

Abstract: This research proposes a roof-mounted auxiliary power supply (APS) system for 600VDC low-floor light rail vehicle (LRV). The proposed APS system consists of five parallel-connected dc-ac inverter modules (modules 1-5). The inverter modules 1 and 2 are three-phase dc-ac inverters for compressor motors of the cooling system, and the inverter modules 3 and 4 are three-phase dc-ac inverters for air pump motors of the braking system. The inverter module 5 is single-phase dc-ac inverter for 220VAC power supply for onboard electric loads. Simulations and experiments were carried out under variable load torque and output frequency for modules 1 – 4; and under full and no resistive loads for the inverter module 5. The measured total input current and total input power of the proposed APS system under full load condition are 118.76A and 71.25kW. Essentially, the proposed APS system is operationally applicable to the 600VDC low-floor RLV. Besides, the novelty of this research lies in the use of five parallel-connected inverter modules, unlike in the conventional APS systems which require three-phase output transformer or isolated dc-dc converter. Specifically, the proposed APS system requires neither three-phase output transformer nor isolated dc-dc converter.

Keywords: auxiliary power supply system; low-floor light rail vehicle; dc train; parallel-connected dc-ac inverter; variable voltage variable frequency control

1. Introduction

Metropolises and large cities around the world combat urban traffic congestion and air pollution by constructing and encouraging the use of public transportation, particularly dc trains. Examples of dc trains are tramway [1,2], light rail vehicle [3–5], metro [6–8], and subway [9]. Of particular interest is light rail vehicle (LRV) which is a type of dc train suitable for passenger transportation in less densely populated urban areas (i.e., second- or third-tier cities).

The main components of the propulsion system of LRV include bogie [10], car body [11], traction motor [12,13], traction inverter [14], pantograph [15], traction control, network control, and braking system. Besides, there are onboard components for train passenger comfort, such as the cooling system [16], auxiliary power supply system, electric doors, and air suspension.

Auxiliary power supply (APS) system is an onboard electrical power supply system which is mounted on the roof for low-floor LRV or underfloor for high-floor LRV [17–31]. The APS system converts high-voltage power from a dc traction substation [32] supplied through the overhead contact line and pantograph into three-phase and single-phase ac voltage power for onboard electric loads, such as the cooling system, air pumps, lighting, electric doors, and battery charging system.

The early APS system consists of input filter circuit, dc-ac inverter, and three-phase output transformer. The advantage of the early APS system is pure sinusoidal output waveform. However, the early APS system suffers from heavy weight and bulkiness. Figure 1 shows the early APS system

Preprints (www.preprints.org) | NOT PEER-REVIEWED | Posted: 1 May 2023 doi:10.20944/preprints202305.0020.v1

for dc trains. The main components include the input filter circuit to reduce input voltage ripple, the dc-ac inverter to invert dc voltage into three-phase ac voltage power in the form of three-phase modified sinusoidal waveform, and the three-phase output transformer to transform the three-phase modified to pure sinusoidal waveform and single-phase 220VAC. A rectifier circuit converts single-phase 220VAC into 24VDC or 110VDC for battery charging and control system. Due to the heavy weight and bulkiness of the early APS system, the technology is limited to underfloor installation in high-floor LRV.

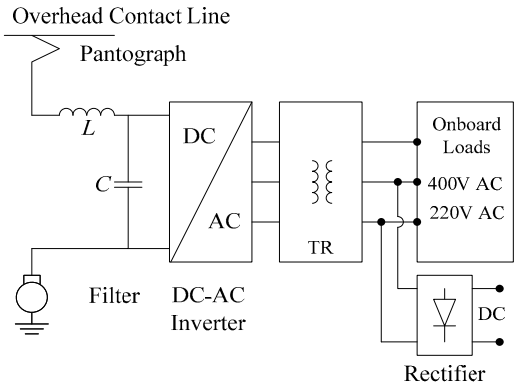

Figure 1. The early auxiliary power supply system with three-phase output transformer for dc trains.

Figure 2 shows the APS system with isolated dc-dc converter and high-frequency transformer for DC trains. In the figure, the three-phase output transformer is replaced by the dc-dc converter to reduce the size and weight of the APS system. Existing research on the APS system with isolated dc-dc converter for dc trains can be categorized into three groups based on the overhead contact line voltage: 3000VDC, 750-1500VDC, and 600VDC.

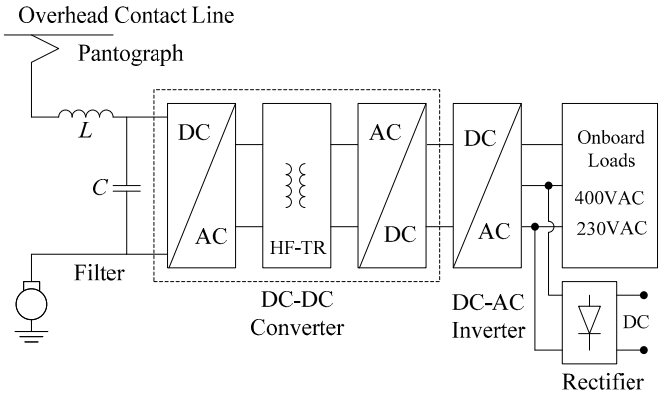

Figure 2. The isolated dc-dc converter with high-frequency transformer of the APS system for dc trains.

The first group is the APS system for dc trains with 3000VDC nominal overhead contact line voltage [17–21]. In [17], the 235kW APS system with dual dc-dc converter isolates and converts the overhead contact line voltage, varying between 2.1kV – 4.7kV, into 600VDC for dc trains in Russia. In [18], the APS system with front-end isolated dc-dc converter for multi-current locomotives is operable in both 16 2/3Hz 15kVAC and 3.0kVDC trains in European countries. To overcome the size and weight of the APS for 3.0KV dc commuter trains, the high-frequency output transformer in the isolated dc-dc converter is replaced with the low-frequency output transformer [19] and the number of series-connected IGBTs of the isolated dc-dc converter is reduced [20,21].

The second group is the APS system for 750VDC and 1500VDC trains using IGBT power modules [22–24] and SiC MOSFET power modules [25–28] in the isolated dc-dc converters. In [22],

 doi:10.20944/preprints202305.0020.v1

the APS system was proposed for 1500VDC double-deck dc trains in the Netherlands, whereby 500VDC output voltage of the dc-dc converter is for the cooling system and 380VAC from the dc-ac inverter for the air pump motors and onboard electric loads. The three-phase dual active bridge dc-dc converter [23] and the three-level soft switching dc-dc converter [24] are deployed in the APS systems for 750VDC overhead contact line dc trains. To increase efficiency and power density of the dc-dc converter, the IGBT power modules are replaced with the SiC MOSFET modules [25–28].

The last group is the APS system with isolated dc-dc converter for 600VDC trains [29,30]. In [29], the soft-switching topology of the dc-dc converter is proposed to reduce the number of diodes, IGBT modules, weight, and size of the APS system. In [30], the pulse width modulation-voltage source inverter (PWM-VSI) over-modulation technique of dc-ac inverter is used to reduce total harmonic distortion of the APS system due to variation in the overhead contact line voltage. In [31], the authors comparatively investigate the switching losses and output efficiency of the dc-dc converters of APS with IGBT power module and SiC MOSFET power module. The isolated dc-dc converter circuit is conventionally used in the APS system. Nevertheless, if the dc-dc converter circuit is faulty, the propulsion system and the APS system will stop functioning, resulting in train service disruptions.

Specifically, this research proposes a roof-mounted APS system for 600VDC low-floor light rail vehicle. The proposed APS system consists of five parallel-connected inverter modules (modules 1 – 5), as shown in Figure 3. The inverter modules 1 and 2 are three-phase dc-ac inverters for compressor motors of the cooling system, and modules 3 and 4 are three-phase dc-ac inverters for air pump motors of the braking system. The inverter module 5 is single-phase dc-ac inverter for 220VAC power supply for onboard electric loads. Unlike the early APS system and the conventional APS system with isolated dc-dc converter, the proposed APS system requires no three-phase output transformer and isolated dc-dc converter. Instead, the proposed APS system utilizes five parallel-connected inverter modules. Besides, simulations and experiments were carried out under variable load torque (25 – 100%) and output frequency (10 – 50Hz) for modules 1 – 4; and under full resistive load and no resistive load for inverter module 5. The performance metrics are total input current and total input power of the proposed APS system (modules 1 – 5) under full load condition.

The organization of this research is as follows: Section 1 is the introduction. Section 2 details the roof-mounted auxiliary power supply system of low-floor LRV. Section 3 deals with the development of the proposed APS system for low-floor LRV. Section 4 discusses the simulation and experimental results of the proposed APS system. The concluding remarks are provided in Section 5.

Preprints (www.preprints.org) | NOT PEER-REVIEWED | Posted: 1 May 2023 doi:10.20944/preprints202305.0020.v1

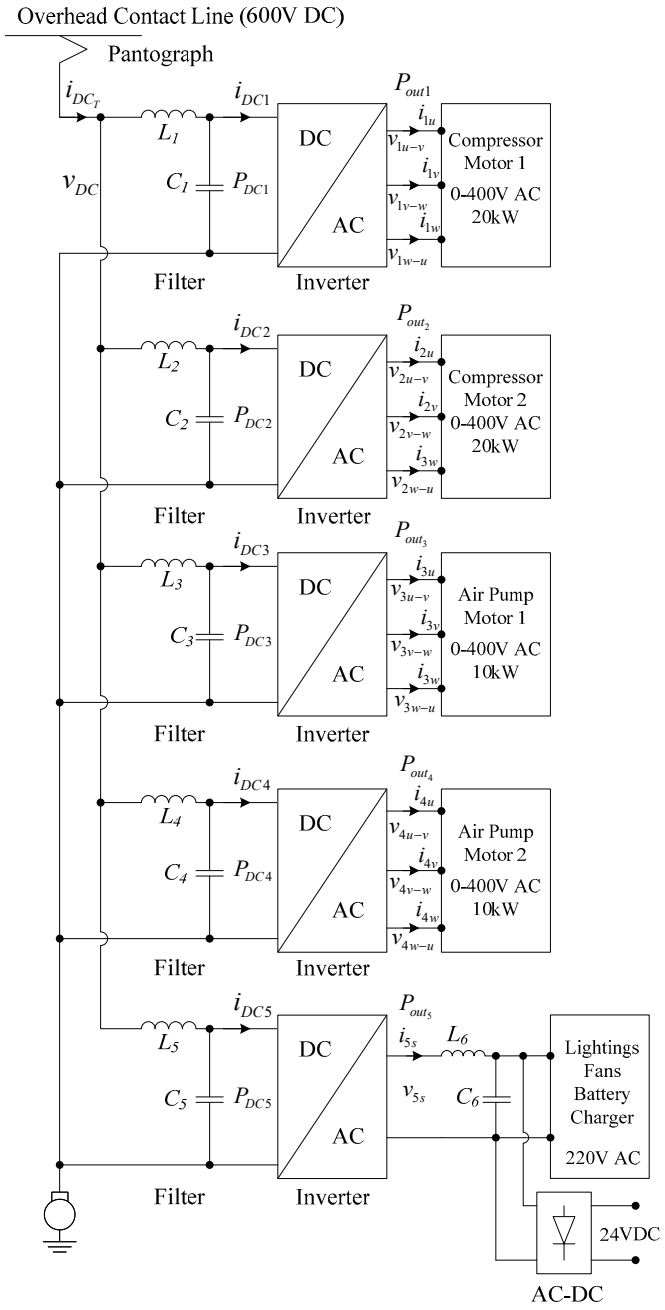

Figure 3. Proposed auxiliary power supply system for 600VDC low-floor light rail vehicle.

2. Roof-Mounted Auxiliary Power Supply System

2.1. Overhead Contact System of Low-Floor Light Rail Vehicle

The overhead contact system (OCS) is the power distribution system that delivers power to a light rail vehicle (LRV) from a contact wire. In this research, the OCS of low-floor LRV includes the overhead contact wire (i.e. 600VDC overhead contact line), messenger wire, dropper, support poles and power feeds from DC traction substation to the overhead contact wire, as shown in Figure 4. The voltage range and maximum traction power of the DC traction substation are 540 – 800VDC and 2x500kW, respectively.

Preprints (www.preprints.org) | NOT PEER-REVIEWED | Posted: 1 May 2023 doi:10.20944/preprints202305.0020.v1

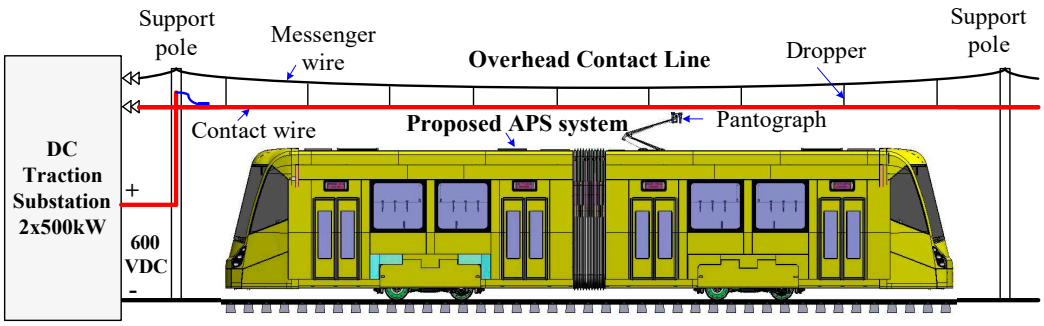

Figure 4. The 600VDC overhead contact line for the proposed APS system of the low-floor LRV.

2.2. Connecting Diagram of Roof-Mounted Auxiliary Power Supply System

Figure 5(a) shown the 3D model of a low-floor LRV with two cars connected by an articulation joint. In Figure 5(b), the proposed APS system is mounted on the rooftop of car no. 1 together with traction inverter and cooling system. On the rooftop of car no. 2 are installed a pantograph, the traction inverter and the cooling system.

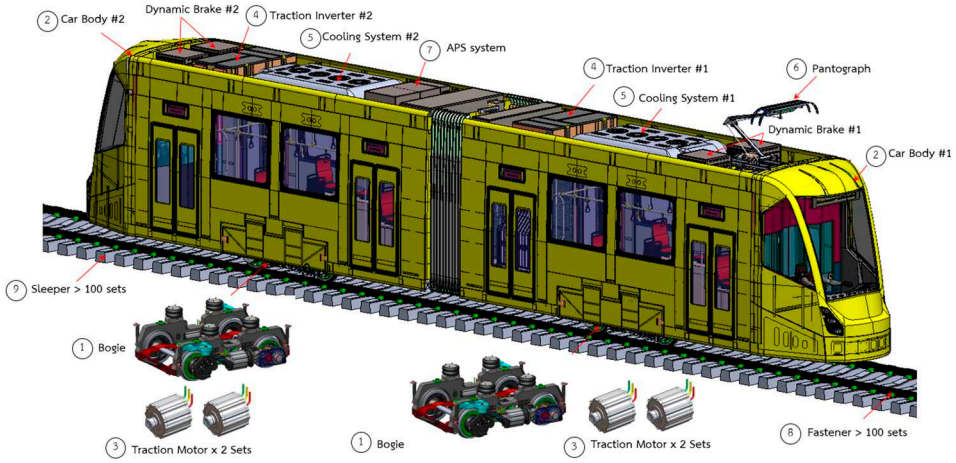

(a)

(b)

Figure 5. The 600VDC low-floor LRV with the proposed APS system: (a) 3D model, (b) roof-mounted electric parts on top of car no. 1 and 2.

Figure 6 shows the connecting diagram of the proposed APS system and onboard electric loads between car no. 1 and 2 of the low-floor LRV. On the rooftop of car no. 1 are installed the pantograph,

Preprints (www.preprints.org) | NOT PEER-REVIEWED | Posted: 1 May 2023 doi:10.20944/preprints202305.0020.v1

the lighting arrester (LA), the main circuit breaker (MCB), traction inverter #1, and cooling system #1. On the rooftop of car no. 2 are mounted traction inverter #2, cooling system #2, and the APS system.

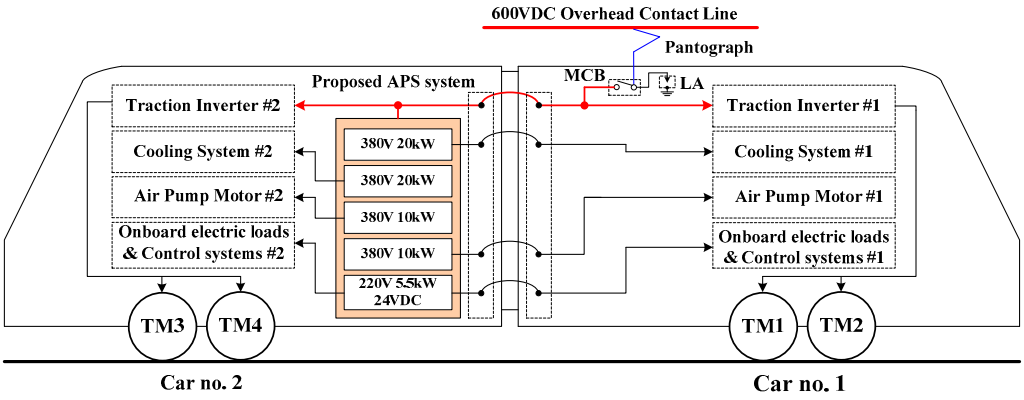

Figure 6. Connecting diagram of the proposed APS system and onboard electric loads on the low-floor LRV.

2.3. Power Consumption of Auxiliary Power Supply System in Light Rail Vehicle

The total input power of the APS system (P_{DCT}) is calculated by multiplying the dc voltage of the overhead contact line (v_{DC}) multiply with the total dc input current (i_{DCT}) and can be mathematically expressed as:

$$P_{DCT} = v_{DC} i_{DCT}, \tag{1}$$

$$i_{DCT} = i_{DC1} + i_{DC2} + i_{DC3} + i_{DC4} + i_{DC5}, \tag{2}$$

$$P_{DCT} = v_{DC}(i_{DC1} + i_{DC2} + i_{DC3} + i_{DC4} + i_{DC5}), \tag{3}$$

$$P_{DCT} = P_{DC1} + P_{DC2} + P_{DC3} + P_{DC4} + P_{DC5}, \tag{4}$$

where P_{DCT} is the total input power, v_{DC} is the overhead contact line voltage, i_{DCT} is the total input current of APS, i_{DC1} and i_{DC2} are the input current of the dc-ac inverters for the compressor motor no. 1 and 2, i_{DC3} and i_{DC4} are the input current of the dc-ac inverters for air pump motor no. 3 and 4, i_{DC5} is the input current of the dc-ac inverter for the single-phase power supply, P_{DC1} and P_{DC2} are the input power of the dc-ac inverters for compressor motor no. 1 and 2, P_{DC3} and P_{DC4} are the input power of the dc-ac inverters for air pump motor no. 3 and 4, and P_{DC5} is the input power of the dc-ac inverter for single-phase power supply.

2.4. Variable Voltage and Variable Frequency Control Method

In this research, the variable voltage variable frequency (VVVF) control method is utilized to vary the speed of the three-phase compressor motors of the cooling system and the three-phase air pump motors of the braking system of the low-floor LRV. Specifically, the speed of the compressor and air pump motors are regulated by varying the stator voltage and output frequency. The advantages of the VVVF controller include straightforwardness, low-complexity algorithm, and ease of implementation. The relationship between the stator voltage, output frequency, air gap flux, and maximum torque of induction motor can be mathematically expressed as:

$$v_s = \left(\frac{v}{f}\right) f_s, \tag{5}$$

$$v_s = \frac{2\pi}{\sqrt{2}} N_C k_p \emptyset f_s, \tag{6}$$

$$\emptyset = \frac{v_s}{\left[\frac{2\pi}{\sqrt{2}} N_C k_p f_s\right]}, \tag{7}$$

Preprints (www.preprints.org) | NOT PEER-REVIEWED | Posted: 1 May 2023 doi:10.20944/preprints202305.0020.v1

$$T_{max} \approx \left(\frac{v_s}{f_s}\right)^2, \tag{8}$$

where v_s is the stator voltage, N_c is the number of turn per phase of stator windings, k_p is the stator winding factor, $\emptyset$ is the air gap flux, f_s is the output frequency, v/f is the ratio of stator voltage to output frequency, and T_{max} is the maximum torque.

Figure 7 shows the relationship between torque and speed in the VVVF control method. The ratio of stator voltage to output frequency is varied to optimize the torque and speed of the compressor and air pump motors.

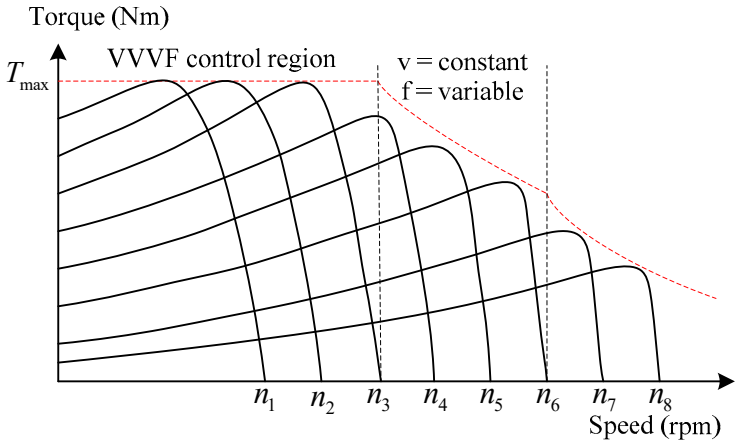

Figure 7. Relationship between torque and speed of the VVVF control method of the compressor and air pump motors.

3. Development of Auxiliary Power Supply System for Low-Floor Light Rail Vehicle

3.1. Development of Three-Phase DC-AC inverter Modules

Figures 8 and 9 show the schematic of the three-phase dc-ac inverters and control diagram of the compressor motors of cooling system (i.e., inverter modules 1 and 2); and the air pump motors of the braking system (inverter modules 3 and 4) of the proposed APS system, respectively. The rated power of the compressor motor drivers (i.e., dc-ac inverters for the compressor motors) and the air pump motor drivers (dc-ac inverters for air pump motors) are 2x20kW and 2x10kW, respectively.

Since the compressor motors and the air pump motors are of three-phase induction motors, this research uses the VVVF controller to controls the speed of the compressor and air pump motors. In this research, the command frequency (f_c) is 50Hz. The stator voltage (v_s) is first derived from the relationship between stator voltage and output frequency using equation (5) and then converted into two-phase quantity as:

$$v_x = v_s cos\omega t, \tag{9}$$

$$v_y = v_s sin\omega t, \tag{10}$$

where v_x is the voltage in x axis and v_y is the voltage in y axis.

The stator voltage in two-phase quantity are converted to three-phase coordinates by inverse Clarke transform method. The three-phase command voltage are mathematically expressed as:

$$v_a = v_x, \tag{11}$$

$$v_b = -\frac{1}{2}v_x + \frac{\sqrt{3}}{2}v_y, \tag{12}$$

$$v_c = -\frac{1}{2}v_x - \frac{\sqrt{3}}{2}v_y, \tag{13}$$

Preprints (www.preprints.org) | NOT PEER-REVIEWED | Posted: 1 May 2023 doi:10.20944/preprints202305.0020.v1

where v_a is the command voltage in phase A, v_b is the command voltage in phase B, and v_c is the command voltage in phase C.

The space vector pulse width modulation (SVPWM) technique is used to generate gate driving signals for IGBTs in the three-phase dc-ac inverters for the compressor and air pump motors.

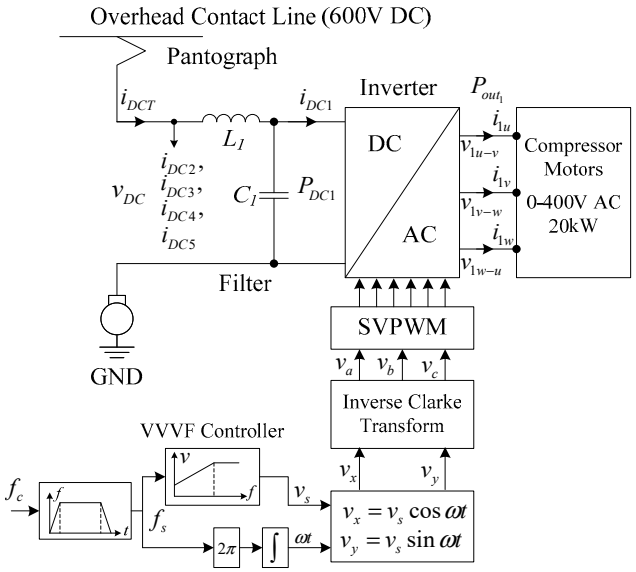

Figure 8. Schematic of three-phase dc-ac inverters and control diagram of the compressor motors of the APS system.

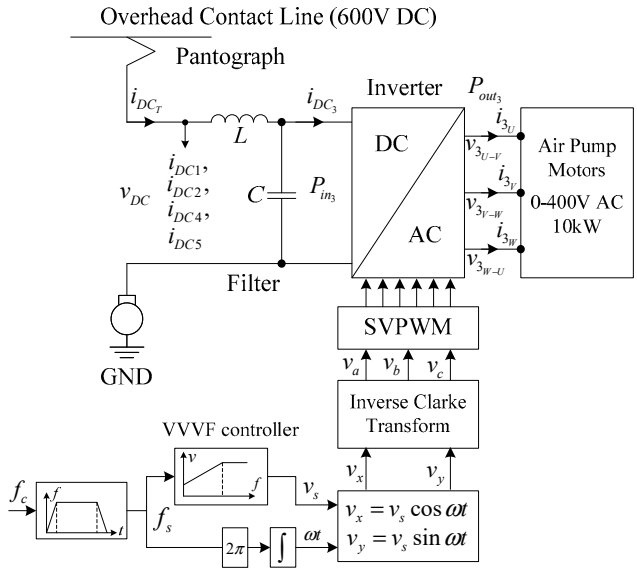

Figure 9. Schematic of three-phase dc-ac inverters and control diagram of the air pump motors of the APS system.

3.2. Development of Single-Phase DC-AC inverter Module

A 220VAC 50Hz single-phase power supply is required to power onboard electric loads such as lighting, fans, CCTV cameras, electric doors, and 24VDC battery charging system. Figure 10 illustrates the magnitude control diagram of the dc-ac inverter for single-phase power supply (i.e., inverter module 5).

The operation principle of the inverter module 5 is as follows:

1. The input command voltage (v_1) is 220VAC;

Preprints (www.preprints.org) | NOT PEER-REVIEWED | Posted: 1 May 2023 doi:10.20944/preprints202305.0020.v1

2. The input command voltage (v_1) is compared against the amplitude of the measured output voltage (v_z) and the difference between voltage v_1 and v_z (Δv) is manipulated by the proportional-integral (PI) controller. The feed forward voltage (v_2) is the summation of v_1 and Δv and is mathematically expressed as;

$$v_2 = v_1 + \Delta v, \tag{11}$$

3. The command frequency (f_1) is 50Hz and through the integrator the angular speed (ω) and time (t) are obtained;

4. The overhead contact line voltage (v_{DC}) is converted to single-phase 220VAC (i.e., the output voltage of the dc-ac inverter) by SVPWM with v_2, ω and t as the inputs;

5. The output voltage of the dc-ac inverter is converted into sinusoidal waveform by using LC low pass filter.

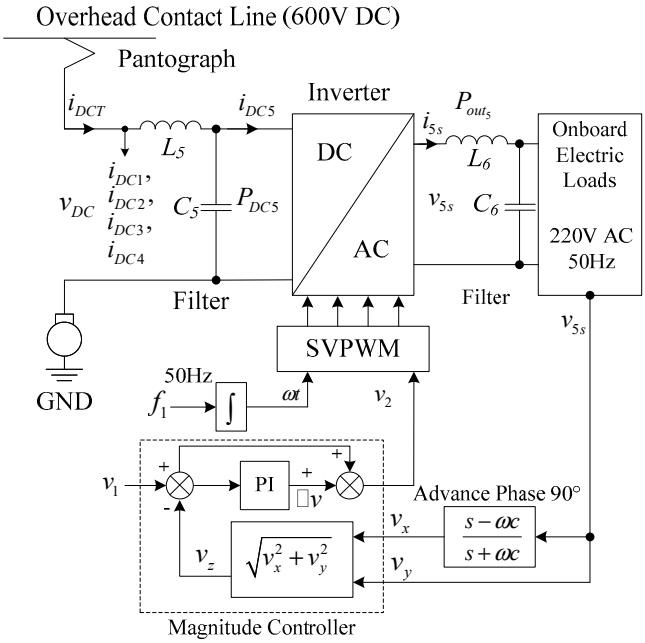

Figure 10. Magnitude control diagram of the single-phase power supply of the proposed APS system.

4. Experimental Results of Auxiliary Power Supply System

The performance of the proposed APS system for low-floor LRV is evaluated under variable load torque (25 – 100%) and output frequency (10 – 50Hz) for the three-phase dc-ac inverter modules for the compressor motors (modules 1 and 2) and the air pump motors (modules 3 and 4). Meanwhile, the performance of the dc-ac inverter for single-phase 220VAC power supply (module 5) is evaluated under full load (resistive load = 100%) and no load (resistive load = 0%). Table 1 tabulates the specifications of the onboard electric loads on low-floor LRV.

Table 1. The specifications of onboard electric loads on low-floor LRV.

Onboard Electric Loads		Details
Compressor motors	Load type	3-phase induction motor
	Output voltage	0 – 400V
	Output frequency	0 – 50Hz
	Rated power	20kW
Air pump motors	Load type	3-phase induction motor
	Output voltage	0 – 400V
	Output frequency	0 – 50Hz

 doi:10.20944/preprints202305.0020.v1

	Rated power	10kW
Lighting,	Load type	1-phase
fans,	Output voltage	220V
electric doors,	Output frequency	50Hz
and battery charging system	Rated power	5.5kW

4.1. Experimental Setup

Figure 11 shows the schematic of the proposed APS system for low-floor LRV, consisting of five dc-ac inverter modules. Specifically, the proposed APS system comprises two 20kW three-phase dc-ac inverter modules for the compressor motors (inverter modules 1 and 2), two 10kW three-phase dc-ac inverter modules for the air pump motors (inverter modules 3 and 4), and one 5.5kW dc-ac inverter for single-phase 220VAC power supply (inverter module 5).

Preprints (www.preprints.org) | NOT PEER-REVIEWED | Posted: 1 May 2023 doi:10.20944/preprints202305.0020.v1

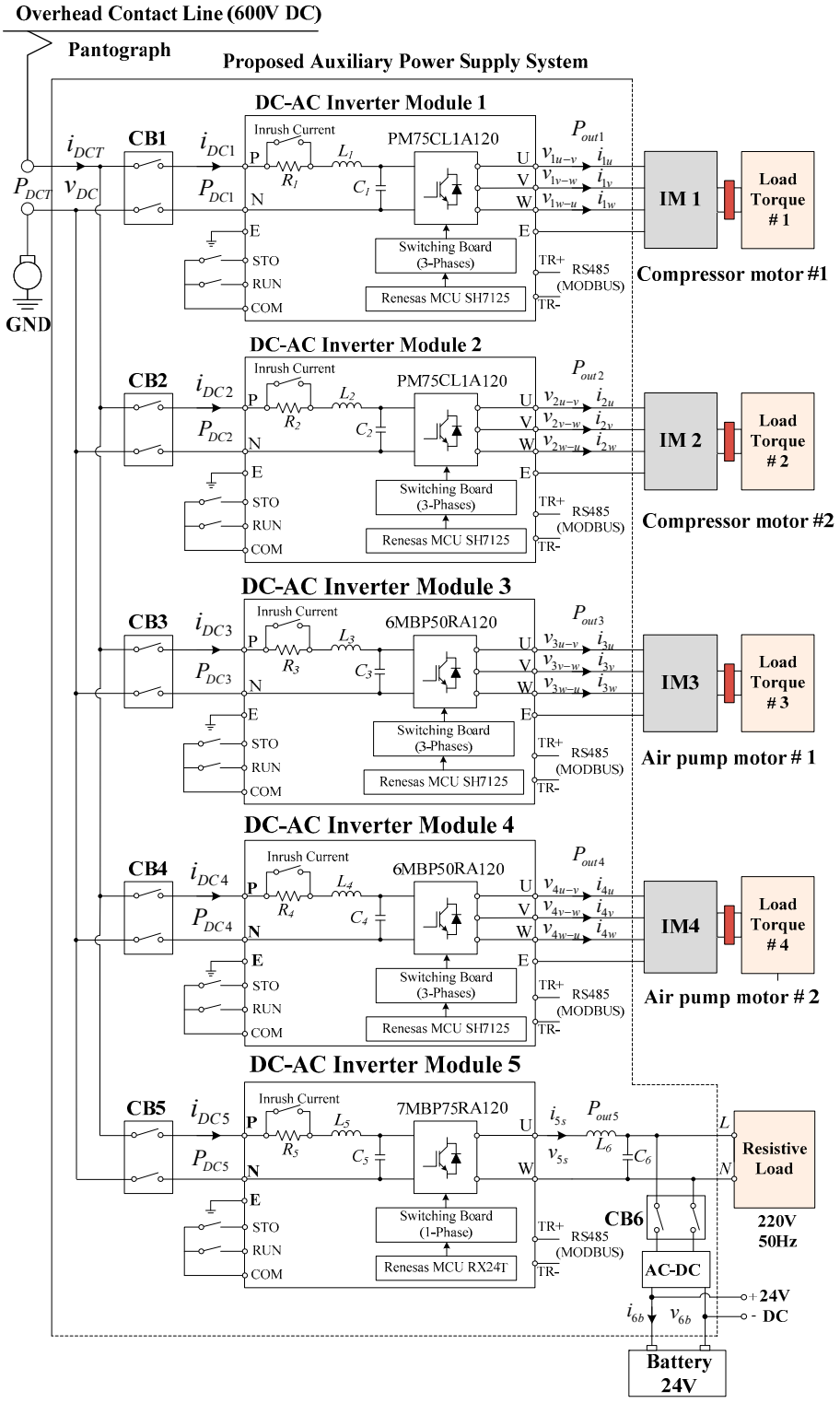

Figure 11. Schematic diagram of the proposed APS system for low-floor LRV.

The 20kW three-phase dc-ac inverter for the compressor motors (i.e., inverter modules 1 and 2) consist of a 100A DC circuit breaker (CB), inrush current limiter, LC low-pass filter, IGBT switches, three-phase switching board (APY Engineering Co., Ltd.), and microcontroller unit (MCU; SH7125, Renesas). The inrush current limiter is used to limit the initial larger flow of electric charge to the capacitor (*C*), and the LC low-pass filter is used to reduce the ripple of overhead contact line voltage (v_{DC}). The IGBT switches are of 75A 1200V switches (PM75CL1A120, Mitsubishi Electric, Japan).

Preprints (www.preprints.org) | NOT PEER-REVIEWED | Posted: 1 May 2023 doi:10.20944/preprints202305.0020.v1

The input power of the inverter module 1 (P_{DC1}) is equal to the overhead contact line voltage (v_{DC}) multiplied by the input current (i_{DC1}). The three-phase output voltage and output current of the inverter module 1 are v_{1u-v}, v_{1v-w}, v_{1w-u}, and i_{1u}, i_{1v}, i_{1w}, respectively. The three-phase output power (P_{out1}) of the inverter module 1 is measured by the two-wattmeter method.

Meanwhile, the input power of the inverter module 2 (P_{DC2}) is equal to the overhead contact line voltage (v_{DC}) multiplied by the input current (i_{DC2}). The three-phase output voltage and output current of the inverter module 2 are v_{2u-v}, v_{2v-w}, v_{2w-u}, and i_{2u}, i_{2v}, i_{2w}, respectively. The three-phase output power (P_{out2}) of the inverter module 2 is measured by the two-wattmeter method.

The 10kW three-phase dc-ac inverter for the air pump motors (i.e., inverter modules 3 and 4) consist of a 40A DC circuit breaker (CB), inrush current limiter, LC low-pass filter, IGBT switches, three-phase switching board (APY Engineering Co., Ltd.), and microcontroller unit (MCU; SH7125, Renesas). The inrush current limiter is used to limit the initial larger flow of electric charge to the capacitor (*C*), and the LC low-pass filter is used to reduce the ripple of overhead contact line voltage (v_{DC}). The IGBT switches are of 50A 1200V switches (6MBP50RA120, Mitsubishi Electric, Japan).

The input power of the inverter module 3 (P_{DC3}) is equal to the overhead contact line voltage (v_{DC}) multiplied by the input current (i_{DC3}). The three-phase output voltage and output current of the inverter module 3 are v_{3u-v}, v_{3v-w}, v_{3w-u}, and i_{3u}, i_{3v}, i_{3w}, respectively. The three-phase output power (P_{out3}) of the inverter module 3 is measured by the two-wattmeter method.

The input power of the inverter module 4 (P_{DC4}) is equal to the overhead contact line voltage (v_{DC}) multiplied by the input current (i_{DC4}). The three-phase output voltage and output current of the inverter module 4 are v_{4u-v}, v_{4v-w}, v_{4w-u}, and i_{4u}, i_{4v}, i_{4w}, respectively. The three-phase output power (P_{out4}) of the inverter module 4 is measured by the two-wattmeter method.

The 5.5kW dc-ac inverter for single-phase 220VAC power supply (i.e., inverter module 5) consist of a 40A DC circuit beaker (CB), inrush current limiter, LC low-pass filter, IGBT switches, Three-phase switching board (APY Engineering Co., Ltd.), and microcontroller unit (MCU; RX24T, Renesas). The inrush current limiter is used to limit the initial large flow of electric charge to the capacitor (*C*), and the LC low-pass filter is used to reduce the ripple of overhead contact line voltage (v_{DC}). The IGBT switches are of 75A 1200V switches (7MBP75RA120), Fuji Electric, Japan). A current sensor (L08P050D15), Tamura) is used to measure the output current of the dc-ac inverter. The ac-dc rectifier circuit is used to convert 220VAC 50Hz to 24VDC for electric doors controller and the control system of low-floor LRV.

The input power of the inverter module 5 (P_{DC5}) is equal to the overhead contact line voltage (v_{DC}) multiplied by the input current (i_{DC5}). The output voltage and output current of the inverter module 5 are v_{5s} and i_{5s}. The single-phase output power (P_{out5}) is measured by a wattmeter (WT330, Yokogawa). The RS485 modbus communication ports are used for the centralized control of the inverter modules 1 – 5.

Figure 12 (a) shows the 3D model of the proposed APS system generated by SolidWorks modeling software, consisting of two three-phase compressor motors (inverter modules 1 – 2), two three-phase air pump motors (inverter modules 3 – 4), and one single-phase power supply (inverter module 5). Figure 12(b) depicts the prototype of the proposed APS system, consisting of 2x20kW three-phase compressor motors, 2x10kW three-phase air pump motors, and 5.5kW 220VAC 50Hz single-phase power supply.

Figure 13(a) shows the SolidWorks-generated 3D model of the proposed APS system with metal casings and electrical enclosures as per Ingress Protection (IP) 65 code against intrusion, dust, accidental contact, and water. Figure 13(b) illustrates the prototype of the APS system with metal casings and electric enclosures according to IP65 code. Figure 14 depicts the experimental setup of the proposed APS system.

Preprints (www.preprints.org) | NOT PEER-REVIEWED | Posted: 1 May 2023 doi:10.20944/preprints202305.0020.v1

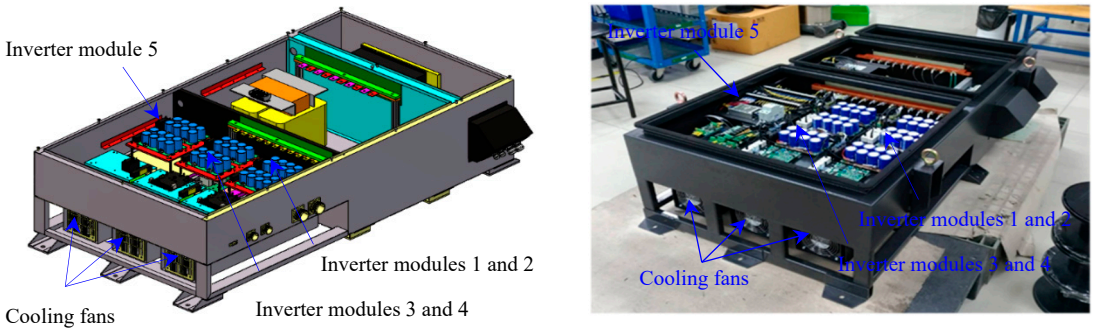

(**a**) (**b**)

Figure 12. The proposed APS system for low-floor LRV consisting of five inverter modules: (**a**) 3D model; (**b**) APS system prototype.

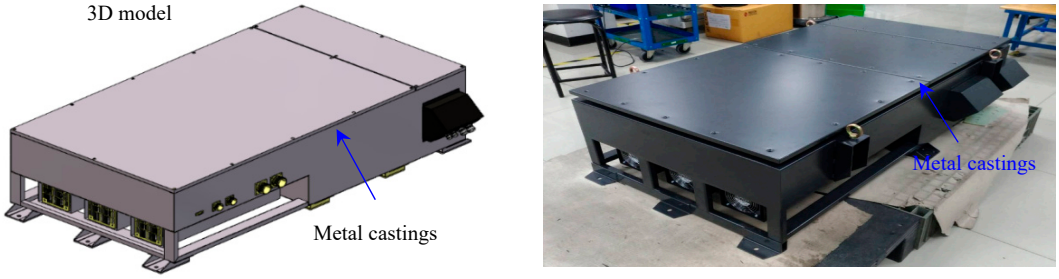

(**a**) (**b**)

Figure 13. The proposed APS system for low-floor LRV with metal castings and electrical enclosures as per IP65 code: (**a**) 3D model; (**b**) APS system prototype with metal castings.

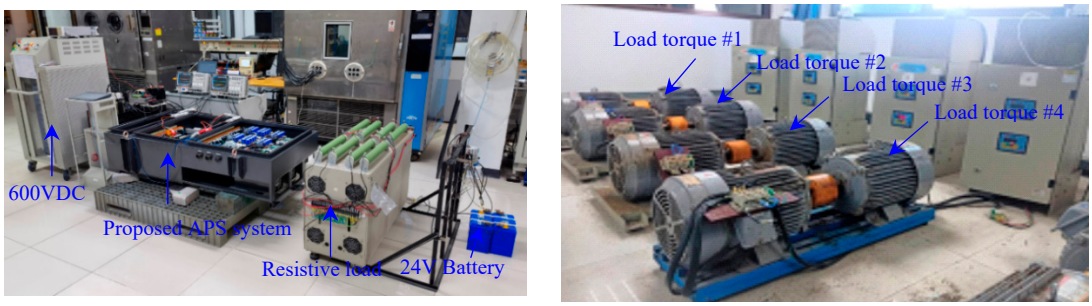

(**a**) (**b**)

Figure 14. The experimental setup of the proposed APS system: (**a**) 600VDC power supply, APS system, resistive load, and 24VDC battery; (**b**) Load torque #1 - #4.

4.2. Simulation and Experimental Results

4.2.1. Three-phase dc-ac Inverters for the compressor motors (inverter modules 1 and 2)

The simulation and experiment of the three-phase dc-ac inverters for the compressor motors of the cooling system (inverter modules 1 and 2) are carried out under the following conditions: (a) the overhead contact line voltage (v_{DC}) is 600VDC; (b) the load torque is varied between 25%, 50%, 75%, and 100%; and (c) the output frequency (f_s) is varied between 10Hz, 20Hz, 30Hz, 40Hz, and 50Hz.

The performance metrics of inverter modules 1 and 2 include (i) the waveforms of input voltage (i.e., overhead contact line voltage; v_{DC}) and of input current of module 1 (i_{DC1}) and module 2 (i_{DC2}); (ii) the waveforms of output voltage (v_{1u-v}, v_{1v-w}, v_{1w-u}) and output current (i_{1u}, i_{1v}, i_{1w}) of module 1 and the waveforms of output voltage (v_{2u-v}, v_{2v-w}, v_{2w-u}) and output current (i_{2u}, i_{2v}, i_{2w}) of module 2; and (iii) the input power of module 1 (P_{DC1}) by multiplying v_{DC} by i_{DC1}, and the input power of module 2 (P_{DC2}) by multiplying v_{DC} by i_{DC2}.

Preprints (www.preprints.org) | NOT PEER-REVIEWED | Posted: 1 May 2023 doi:10.20944/preprints202305.0020.v1

Figure 15 shows, as an example, the simulated and measured waveforms of the three-phase dc-ac inverter for the compressor motor of the cooling system (module 1), given v_{DC}= 600V, f_s= 50Hz, and load torque = 100%. In Figure 15 (a) and (c), the simulated and measured overhead contact line voltage value (v_{DC}) are 600V and 609V, and the simulated and measured output voltage (v_{1u-v}, v_{1v-w}, v_{1w-u}) are 430V, 430V, and 430V; and 433V, 430V, and 439V, respectively. In Figure 15 (b) and (d), the simulated and measured dc input current (i_{DC1}) are 38A and 37.9A; and the simulated and measured output current (i_{1u}, i_{1v}, i_{1w}) are 40A, 40A, and 40A; and 39.9A, 39.7A, and 40.0A, respectively.

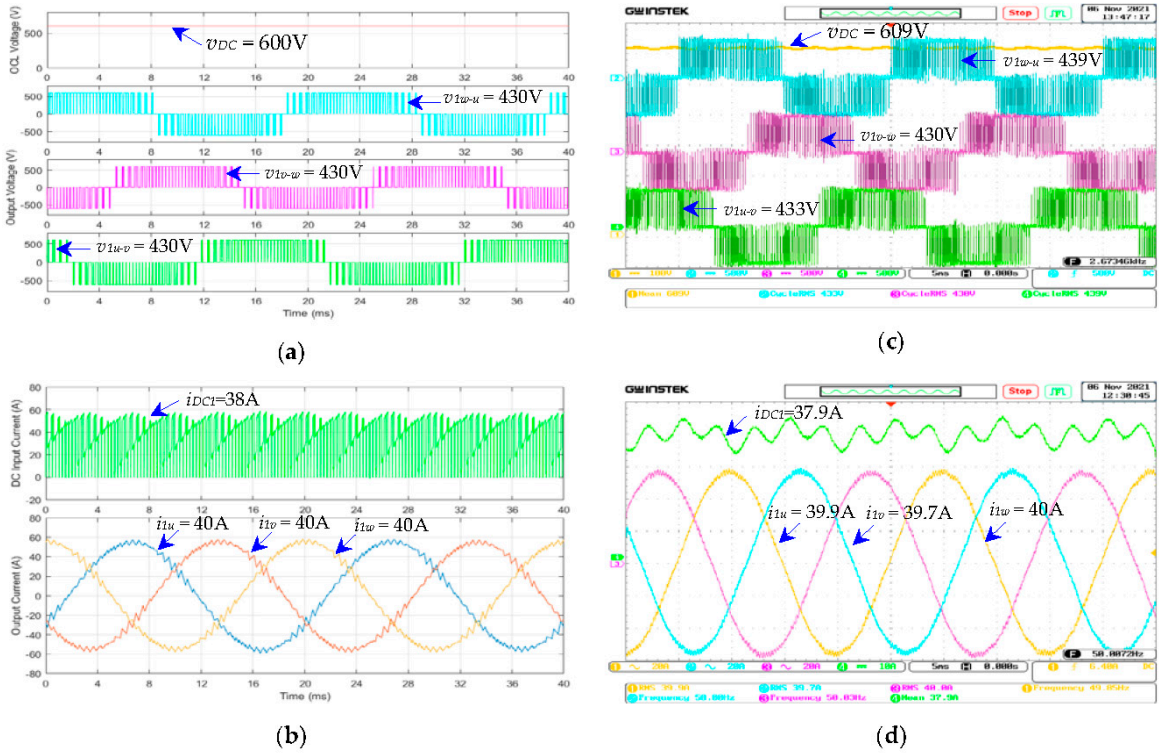

Figure 15. The waveforms of the three-phase dc-ac inverters for the compressor motors (modules 1 and 2): (**a**) simulated v_{DC}, v_{1u-v}, v_{1v-w}, v_{1w-u}; (**b**) simulated i_{DC1}, i_{1u}, i_{1v}, i_{1w}; (**c**) measured v_{DC}, v_{1u-v}, v_{1v-w}, v_{1w-u}; (**d**) measured i_{DC1}, i_{1u}, i_{1v}, i_{1w}; given v_{DC}= 600V, f_s= 50Hz, load torque = 100%.

Figure 16 shows, as an example, the simulated and measured waveforms of the three-phase dc-ac inverter for the compressor motor of the cooling system (module 1), given v_{DC}= 600V, f_s= 50Hz, and load torque = 75%. In Figure 16 (a) and (c), the simulated and measured overhead contact line voltage value (v_{DC}) are 600V and 606V, and the simulated and measured output voltage (v_{1u-v}, v_{1v-w}, v_{1w-u}) are 430V, 430V, and 430V; and 436V, 427V, and 430V, respectively. In Figure 16 (b) and (d), the simulated and measured dc input current (i_{DC1}) are 28A and 28.2A; and the simulated and measured output current (i_{1u}, i_{1v}, i_{1w}) are 30A, 30A, and 30A; and 30.6A, 30.3A, and 30.7A, respectively.

Preprints (www.preprints.org) | NOT PEER-REVIEWED | Posted: 1 May 2023 doi:10.20944/preprints202305.0020.v1

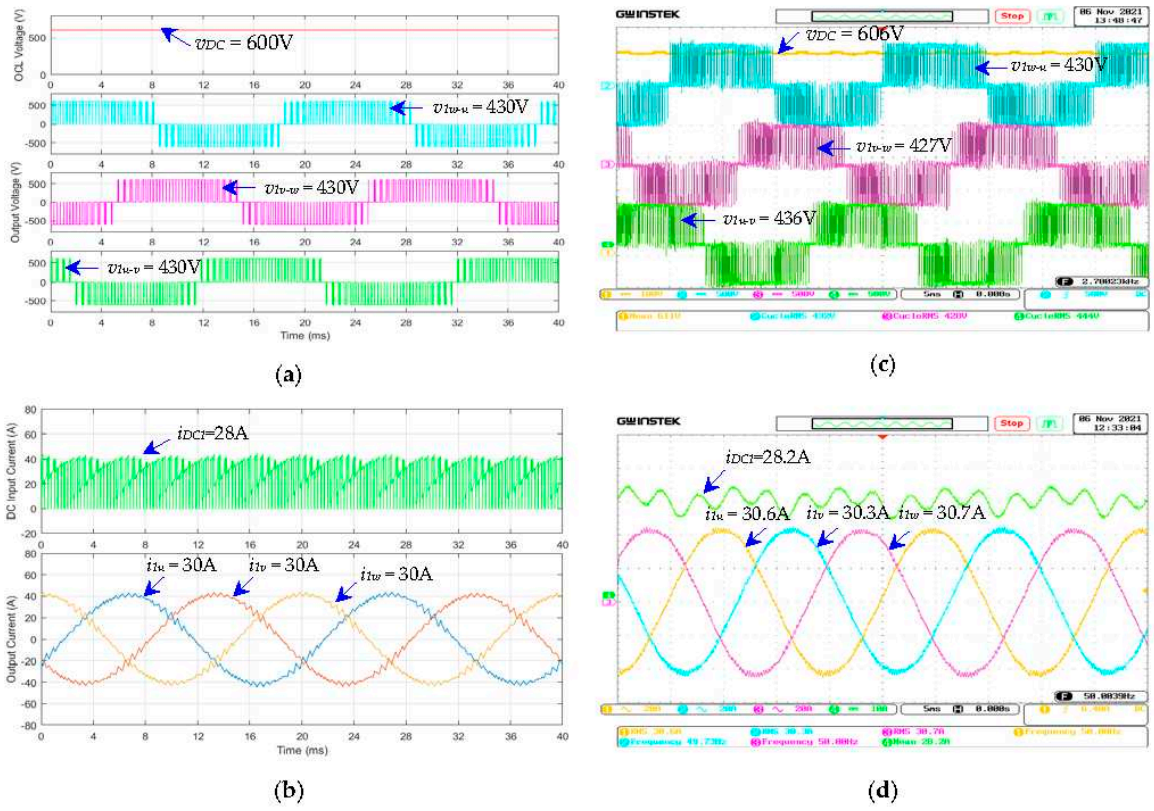

Figure 16. The waveforms of the three-phase dc-ac inverters for the compressor motors (modules 1 and 2): (**a**) simulated v_{DC}, v_{1u-v}, v_{1v-w}, v_{1w-u}; (**b**) simulated i_{DC1}, i_{1u}, i_{1v}, i_{1w}; (**c**) measured v_{DC}, v_{1u-v}, v_{1v-w}, v_{1w-u}; (**d**) measured i_{DC1}, i_{1u}, i_{1v}, i_{1w}; given v_{DC}= 600V, f_s= 50Hz, load torque = 75%.

Figure 17 shows, as an example, the simulated and measured waveforms of the three-phase dc-ac inverter for the compressor motor of the cooling system (module 1), given v_{DC} = 600V, f_s= 50Hz, and load torque = 50%. In Figure 17 (a) and (c), the simulated and measured overhead contact line voltage value (v_{DC}) are 600V and 617V, and the simulated and measured output voltage (v_{1u-v}, v_{1v-w}, v_{1w-u}) are 430V, 430V, and 430V; and 446V, 432V, and 445V, respectively. In Figure 17 (b) and (d), the simulated and measured dc input current (i_{DC1}) are 16A and 16.3A; and the simulated and measured output current (i_{1u}, i_{1v}, i_{1w}) are 20A, 20A, and 20A; and 20.1A, 19.9A, and 20.1A, respectively.

Figure 18 shows, as an example, the simulated and measured waveforms of the three-phase dc-ac inverter for the compressor motor of the cooling system (module 1), given v_{DC}= 600V, f_s= 50Hz, and load torque = 25%. In Figure 18 (a) and (c), the simulated and measured overhead contact line voltage value (v_{DC}) are 600V and 614V, and the simulated and measured output voltage (v_{1u-v}, v_{1v-w}, v_{1w-u}) are 430V, 430V, and 430V; and 434V, 432V, and 441V, respectively. In Figure 18 (b) and (d), the simulated and measured dc input current (i_{DC1}) are 4A and 4.11A; and the simulated and measured output current (i_{1u}, i_{1v}, i_{1w}) are 12A, 12A, and 12A; and 12.9A, 12.7A, and 13.0A, respectively.

The simulated and measured waveforms of both three-phase dc-ac inverters for the compressor motors (i.e., modules 1 and 2) are identical.

Preprints (www.preprints.org) | NOT PEER-REVIEWED | Posted: 1 May 2023 doi:10.20944/preprints202305.0020.v1

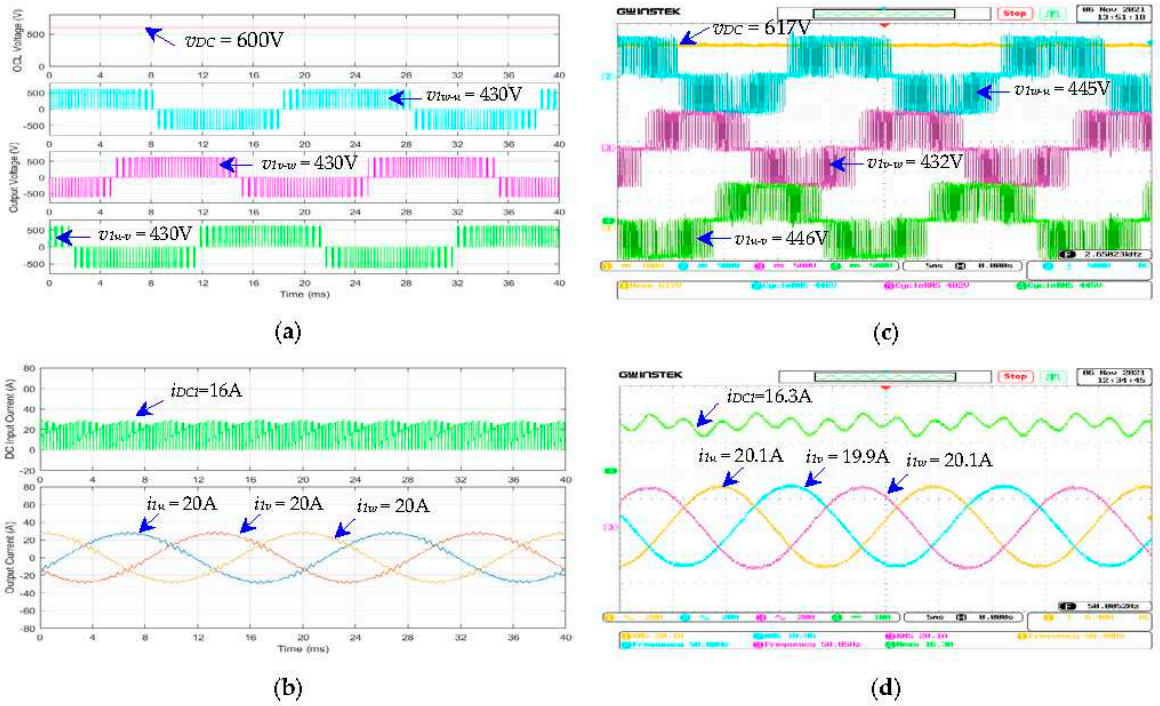

Figure 17. The waveforms of the three-phase dc-ac inverters for the compressor motors (modules 1 and 2): (**a**) simulated v_{DC}, v_{1u-v}, v_{1v-w}, v_{1w-u}; (**b**) simulated i_{DC1}, i_{1u}, i_{1v}, i_{1w}; (**c**) measured v_{DC}, v_{1u-v}, v_{1v-w}, v_{1w-u}; (**d**) measured i_{DC1}, i_{1u}, i_{1v}, i_{1w}; given v_{DC}= 600V, f_s= 50Hz, load torque = 50%.

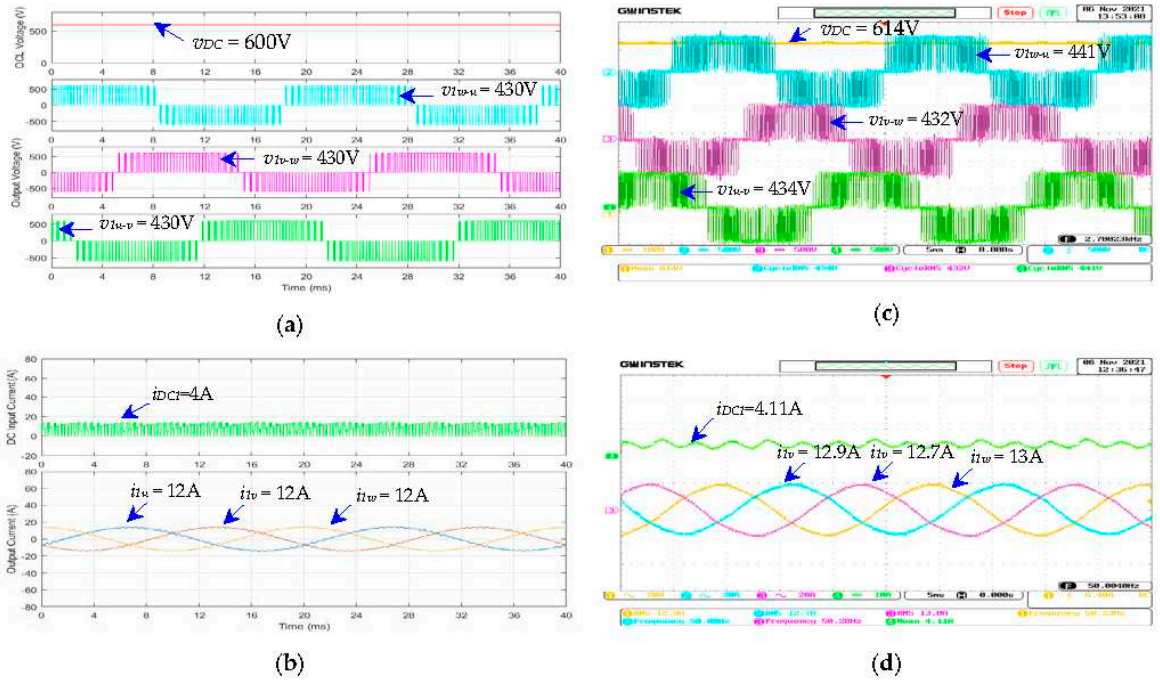

Figure 18. The waveforms of the three-phase dc-ac inverters for the compressor motors (modules 1 and 2): (**a**) simulated v_{DC}, v_{1u-v}, v_{1v-w}, v_{1w-u}; (**b**) simulated i_{DC1}, i_{1u}, i_{1v}, i_{1w}; (**c**) measured v_{DC}, v_{1u-v}, v_{1v-w}, v_{1w-u}; (**d**) measured i_{DC1}, i_{1u}, i_{1v}, i_{1w}; given v_{DC}= 600V, f_s= 50Hz, load torque = 25%.

Figure 19 (a) shows the measured dc input current (i_{DC1}) of the three-phase dc-ac inverter of the compressor motor (module 1) under variable load torques (25 – 100%) and output frequency (10 –

Preprints (www.preprints.org) | NOT PEER-REVIEWED | Posted: 1 May 2023 doi:10.20944/preprints202305.0020.v1

50Hz). The maximum dc input current (i_{DC1}) is 37.9A, given the load torque and output frequency of 100% (full load) and 50Hz.

Figure 19 (b) shows the measured dc input power (P_{DC1}) of the three-phase dc-ac inverter of the compressor motor (module 1) under variable load torques (25 – 100%) and output frequency (10 – 50Hz). The maximum dc input power (P_{DC1}) is 22.74kW, given the load torque and output frequency of 100% (full load) and 50Hz.

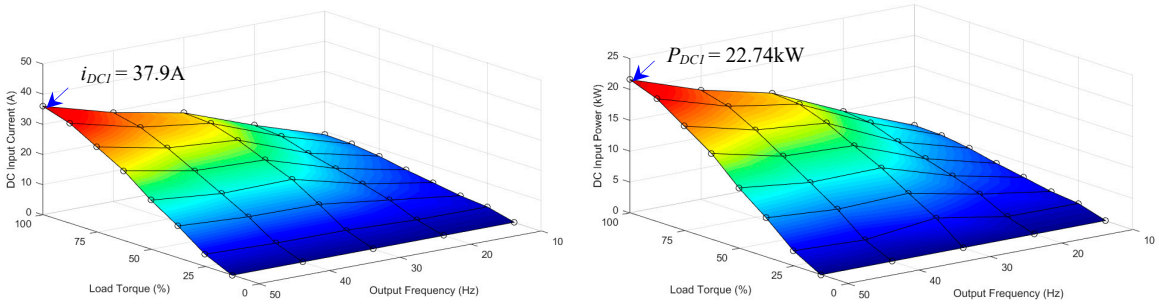

(**a**) (**b**)

Figure 19. The measured results of the three-phase dc-ac inverter for the compressor motors (i.e. module 1) under variable load torque (25 – 100%) and output frequency (10 – 50Hz): (**a**) dc input current (i_{DC1}); (**b**) dc input power (P_{DC1}).

Figure 20 (a) shows the measured dc input current (i_{DC1} and i_{DC2}) of the three-phase dc-ac inverters of the compressor motors (modules 1 and 2) under variable load torques (25 – 100%) and output frequency (10 – 50Hz). The dc input current of modules 1 and 2 (i_{DC1}+i_{DC2}) is 75.8A, given the load torque and output frequency of 100% (full load) and 50Hz.

Figure 20 (b) shows the measured dc input power (P_{DC1} and P_{DC2}) of the three-phase dc-ac inverters of the compressor motors (modules 1 and 2) under variable load torques (25 – 100%) and output frequency (10 – 50Hz). The dc input power of modules 1 and 2 (P_{DC1}+P_{DC2}) is 45.48kW, given the load torque and output frequency of 100% (full load) and 50Hz.

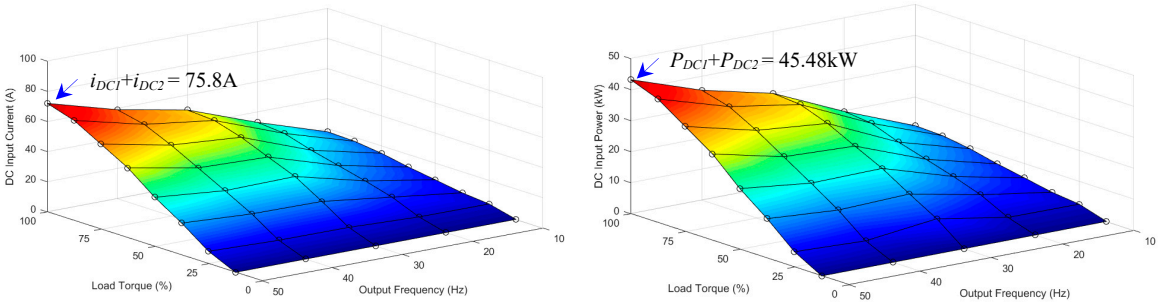

(**a**) (**b**)

Figure 20. The measured results of the three-phase dc-ac inverter for the compressor motors (i.e. modules 1 and 2) under variable load torque (25 – 100%) and output frequency (10 – 50Hz): (**a**) dc input current (i_{DC1}+i_{DC2}); (**b**) dc input power (P_{DC1}+P_{DC2}).

4.2.2. Three-phase dc-ac Inverters for the air pump motors (inverter modules 3 and 4)

The simulation and experiment of the three-phase dc-ac inverters for the air pump motors of the braking system (inverter modules 3 and 4) are undertaken under the following conditions: (a) the overhead contact line voltage (v_{DC}) is 600VDC; (b) the load torque is varied between 25%, 50%, 75%, and 100%; and (c) the output frequency (f_s) is varied between 10Hz, 20Hz, 30Hz, 40Hz, and 50Hz.

The performance metrics of inverter modules 3 and 4 include (i) the waveforms of input voltage (i.e., overhead contact line voltage; v_{DC}) and of input current of module 3 (i_{DC3}) and module 4 (i_{DC4}); (ii) the waveforms of output voltage (v_{3u-v}, v_{3v-w}, v_{3w-u}) and output current (i_{3u}, i_{3v}, i_{3w}) of module 3 and the waveforms of output voltage (v_{4u-v}, v_{4v-w}, v_{4w-u}) and output current (i_{4u}, i_{4v},

Preprints (www.preprints.org) | NOT PEER-REVIEWED | Posted: 1 May 2023 doi:10.20944/preprints202305.0020.v1

i_{4w}) of module 4; and (iii) the input power of module 3 (P_{DC3}) by multiplying v_{DC} by i_{DC3}, and the input power of module 4 (P_{DC4}) by multiplying v_{DC} by i_{DC4}.

Figure 21 shows, as an example, the simulated and measured waveforms of the three-phase dc-ac inverter for the air pump motor of the braking system (module 3), given v_{DC} = 600V, f_s = 50Hz, and load torque = 100%. In Figure 21 (a) and (c), the simulated and measured overhead contact line voltage value (v_{DC}) are 600V and 611V, and the simulated and measured output voltage (v_{3u-v}, v_{3v-w}, v_{3w-u}) are 430V, 430V, and 430V; and 432V, 428V, and 444V, respectively. In Figure 21 (b) and (d), the simulated and measured dc input current (i_{DC3}) are 16A and 16.6A; and the simulated and measured output current (i_{3u}, i_{3v}, i_{3w}) are 14A, 14A, and 14A; and 14.2A, 13.9A, and 14.2A, respectively.

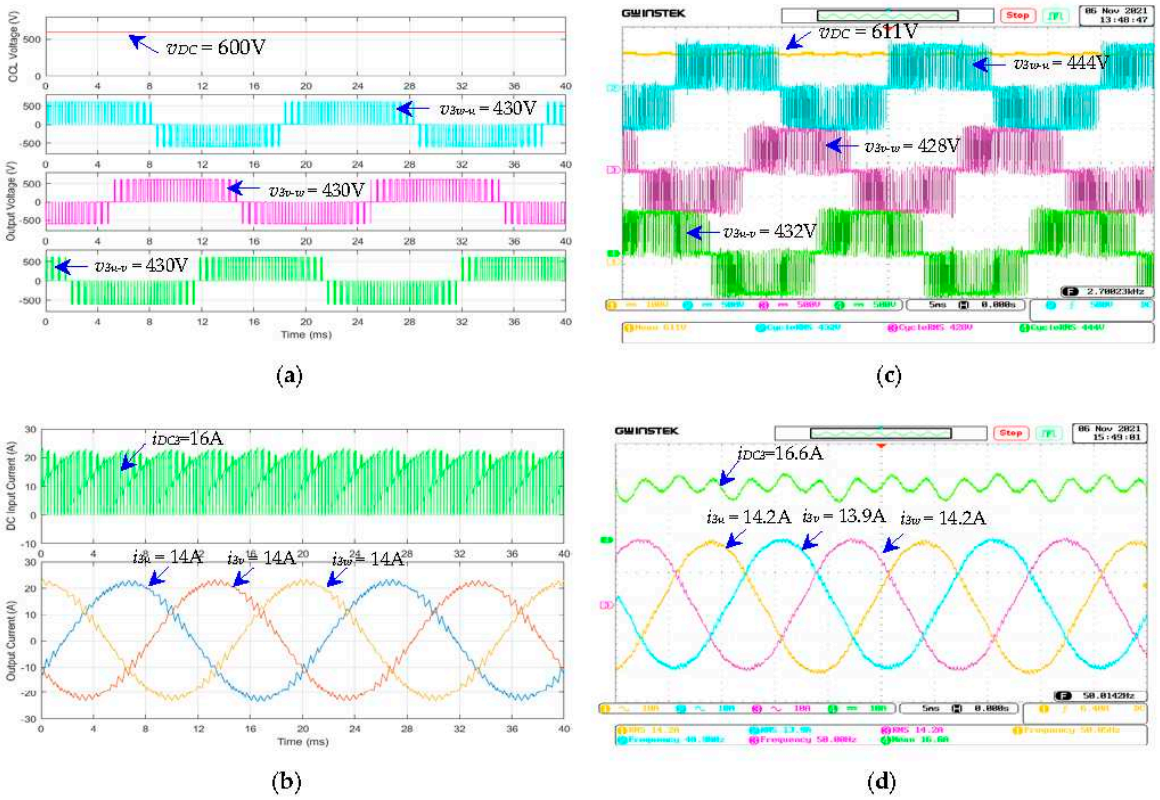

Figure 21. The waveforms of the three-phase dc-ac inverter for the air pump motors (modules 3 and 4): (**a**) simulated v_{DC}, v_{3u-v}, v_{3v-w}, v_{w-u}; (**b**) simulated i_{DC3}, i_{3u}, i_{3v}, i_{3w}; (**c**) measured v_{DC}, v_{3u-v}, v_{3v-w}, v_{w-u}; (**d**) measured i_{DC3}, i_{3u}, i_{3v}, i_{3w}; given v_{DC}= 600V, f_s= 50Hz, load torque = 100%.

Figure 22 shows, as an example, the simulated and measured waveforms of the three-phase dc-ac inverter for the air pump motor of the braking system (module 3), given v_{DC} = 600V, f_s = 50Hz, and load torque = 75%. In Figure 22 (a) and (c), the simulated and measured overhead contact line voltage value (v_{DC}) are 600V and 613V, and the simulated and measured output voltage (v_{3u-v}, v_{3v-w}, v_{3w-u}) are 430V, 430V, and 430V; and 441V, 437V, and 446V, respectively. In Figure 22 (b) and (d), the simulated and measured dc input current (i_{DC3}) are 12A and 11.9A; and the simulated and measured output current (i_{3u}, i_{3v}, i_{3w}) are 10A, 10A, and 10A; and 10.0A, 9.91A, and 10.0A, respectively.

Preprints (www.preprints.org) | NOT PEER-REVIEWED | Posted: 1 May 2023 doi:10.20944/preprints202305.0020.v1

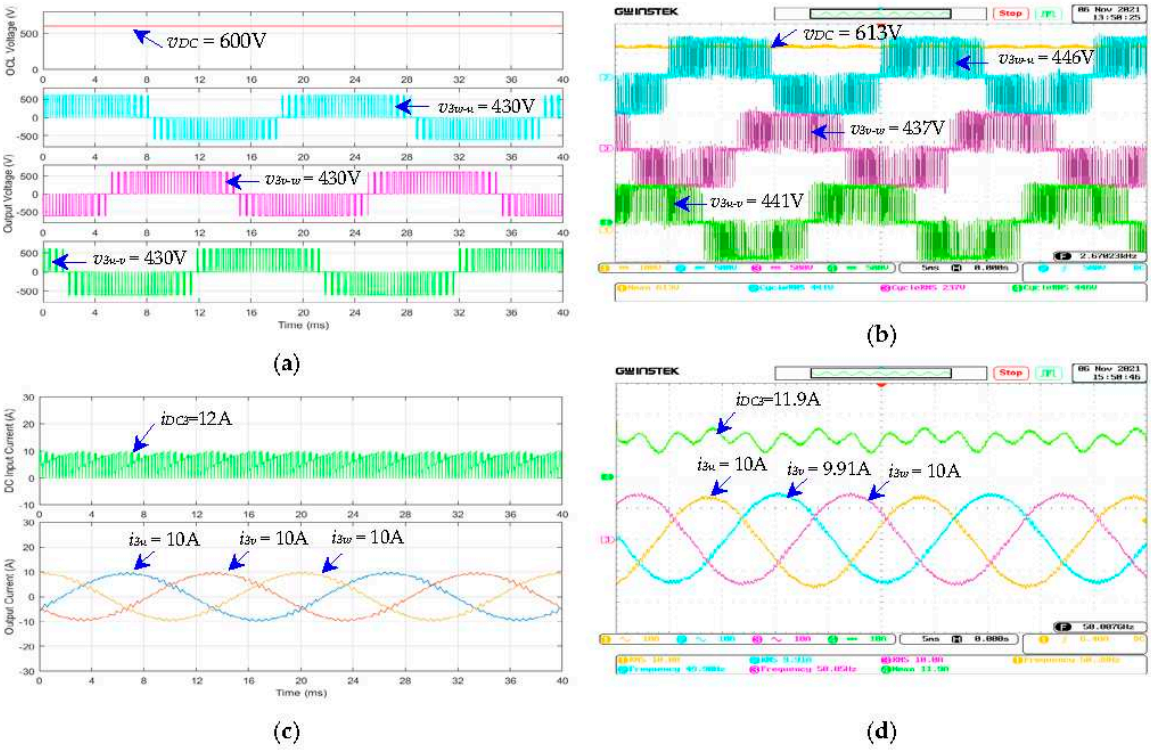

Figure 22. The waveforms of the three-phase dc-ac inverter for the air pump motors (modules 3 and 4): (**a**) simulated v_{DC}, v_{3u-v}, v_{3v-w}, v_{w-u}; (**b**) simulated i_{DC3}, i_{3u}, i_{3v}, i_{3w}; (**c**) measured v_{DC}, v_{3u-v}, v_{3v-w}, v_{w-u}; (**d**) measured i_{DC3}, i_{3u}, i_{3v}, i_{3w}; given v_{DC}= 600V, f_s= 50Hz, load torque = 75%.

Figure 23 shows, as an example, the simulated and measured waveforms of the three-phase dc-ac inverter for the air pump motor of the braking system (module 3), given v_{DC} = 600V, f_s = 50Hz, and load torque = 50%. In Figure 23 (a) and (c), the simulated and measured overhead contact line voltage value (v_{DC}) are 600V and 607V, and the simulated and measured output voltage (v_{3u-v}, v_{3v-w}, v_{3w-u}) are 430V, 430V, and 430V; and 439V, 438V, and 446V, respectively. In Figure 23 (b) and (d), the simulated and measured dc input current (i_{DC3}) are 7A and 7.1A; and the simulated and measured output current (i_{3u}, i_{3v}, i_{3w}) are 6A, 6A, and 6A; and 6.0A, 5.97A, and 6.0A, respectively.

Figure 24 shows, as an example, the simulated and measured waveforms of the three-phase dc-ac inverter for the air pump motor of the braking system (module 3), given v_{DC} = 600V, f_s = 50Hz, and load torque = 25%. In Figure 24 (a) and (c), the simulated and measured overhead contact line voltage value (v_{DC}) are 600V and 617V, and the simulated and measured output voltage (v_{3u-v}, v_{3v-w}, v_{3w-u}) are 430V, 430V, and 430V; and 446V, 442V, and 445V, respectively. In Figure 24 (b) and (d), the simulated and measured dc input current (i_{DC3}) are 2.5A and 2.39A; and the simulated and measured output current (i_{3u}, i_{3v}, i_{3w}) are 3A, 3A, and 3A; and 3.64A, 3.68A, and 3.76A, respectively.

The simulated and measured waveforms of both three-phase dc-ac inverters for the air pump motors (i.e., modules 3 and 4) are identical.

Preprints (www.preprints.org) | NOT PEER-REVIEWED | Posted: 1 May 2023 doi:10.20944/preprints202305.0020.v1

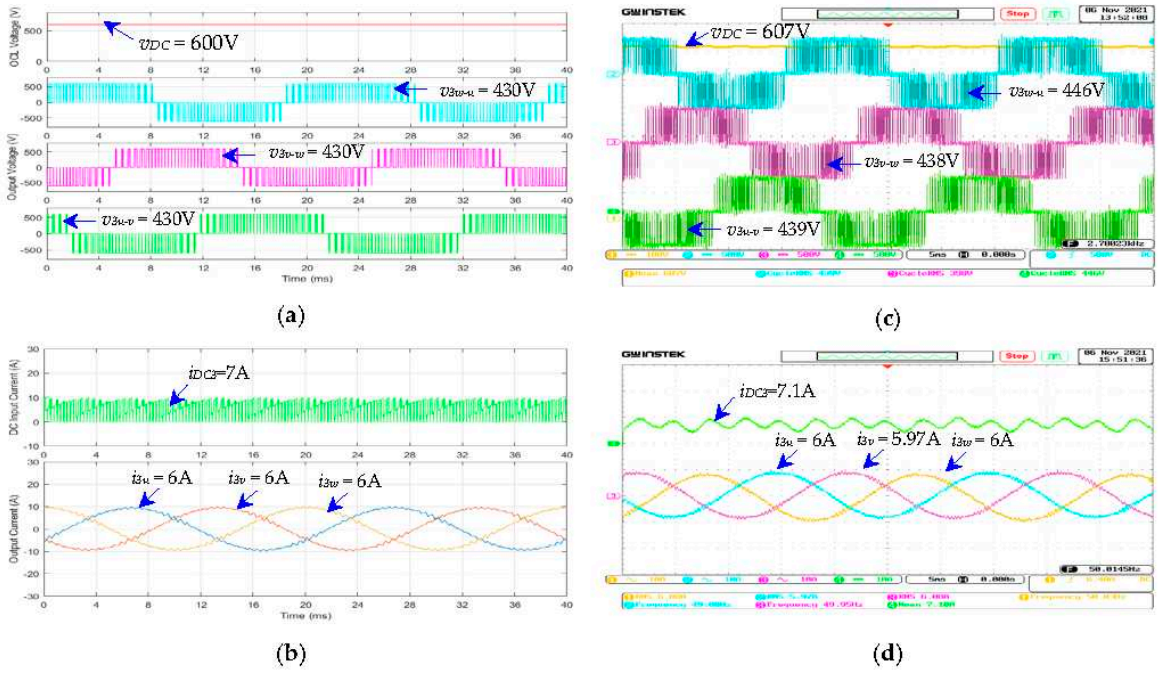

Figure 23. The waveforms of the three-phase dc-ac inverter for the air pump motors (modules 3 and 4): (**a**) simulated v_{DC}, v_{3u-v}, v_{3v-w}, v_{w-u}; (**b**) simulated i_{DC3}, i_{3u}, i_{3v}, i_{3w}; (**c**) measured v_{DC}, v_{3u-v}, v_{3v-w}, v_{w-u}; (**d**) measured i_{DC3}, i_{3u}, i_{3v}, i_{3w}; given v_{DC}= 600V, f_s= 50Hz, load torque = 50%.

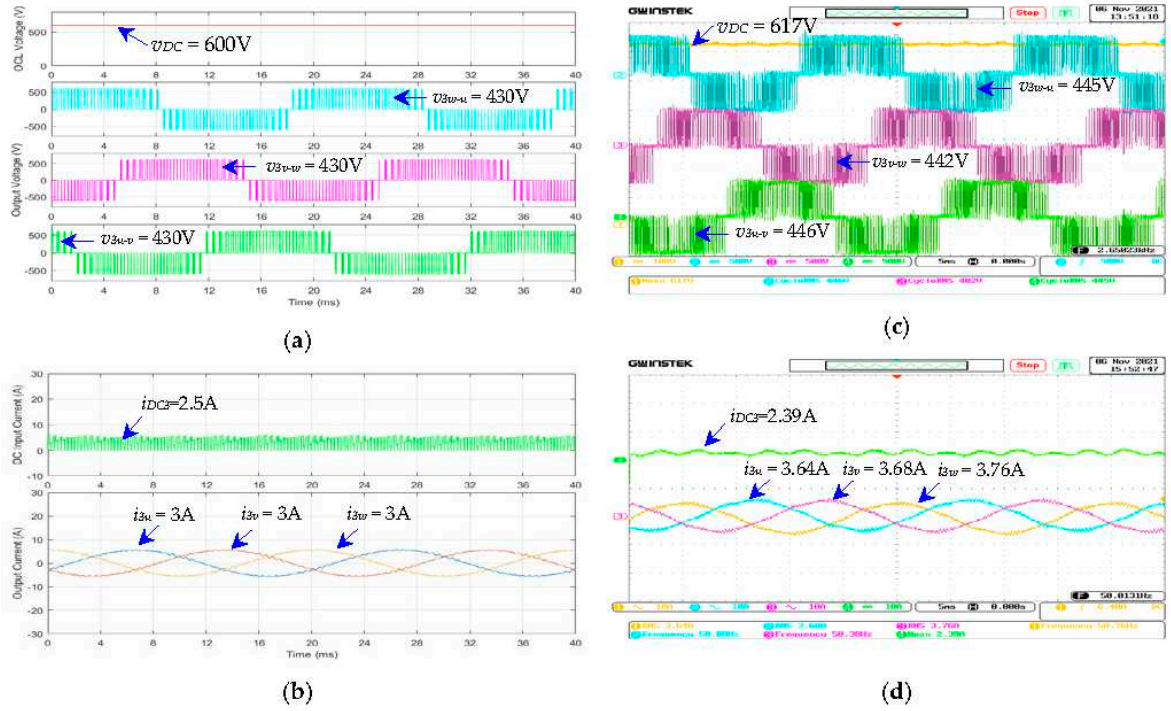

Figure 24. The waveforms of the three-phase dc-ac inverter for the air pump motors (modules 3 and 4): (**a**) simulated v_{DC}, v_{3u-v}, v_{3v-w}, v_{w-u}; (**b**) simulated i_{DC3}, i_{3u}, i_{3v}, i_{3w}; (**c**) measured v_{DC}, v_{3u-v}, v_{3v-w}, v_{w-u}; (**d**) measured i_{DC3}, i_{3u}, i_{3v}, i_{3w}; given v_{DC}= 600V, f_s= 50Hz, load torque = 25%.

Figure 25 (a) shows the measured dc input current (i_{DC3}) of the three-phase dc-ac inverter of the air pump motor (module 3) under variable load torques (25 – 100%) and output frequency (10 – 50Hz). The maximum dc input current (i_{DC3}) is 16.6A, given the load torque and output frequency of 100% (full load) and 50Hz.

Preprints (www.preprints.org) | NOT PEER-REVIEWED | Posted: 1 May 2023 doi:10.20944/preprints202305.0020.v1

Figure 25 (b) shows the measured dc input power (P_{DC3}) of the three-phase dc-ac inverter of the pump motor (module 3) under variable load torques (25 – 100%) and output frequency (10 – 50Hz). The maximum dc input power (P_{DC3}) is 9.96kW, given the load torque and output frequency of 100% (full load) and 50Hz.

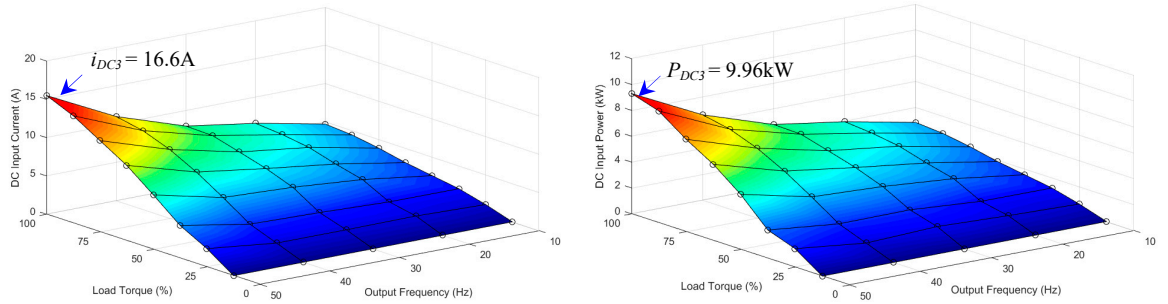

(**a**) (**b**)

Figure 25. The measured results of the three-phase dc-ac inverter for the air pump motors (i.e. modules 3) under variable load torque (25 – 100%) and output frequency (10 – 50Hz): (**a**) dc input current (i_{DC3}); (**b**) dc input power (P_{DC3}).

Figure 26 (a) shows the measured dc input current (i_{DC3} and i_{DC4}) of the three-phase dc-ac inverters of the air pump motors (modules 3 and 4) under variable load torques (25 – 100%) and output frequency (10 – 50Hz). The dc input current of modules 3 and 4 (i_{DC3} + i_{DC4}) is 33.2A, given the load torque and output frequency of 100% (full load) and 50Hz.

Figure 26 (b) shows the measured dc input power (P_{DC3} and P_{DC4}) of the three-phase dc-ac inverters of the air pump motors (modules 3 and 4) under variable load torques (25 – 100%) and output frequency (10 – 50Hz). The dc input power of modules 3 and 4 (P_{DC3} + P_{DC4}) is 19.92kW, given the load torque and output frequency of 100% (full load) and 50Hz.

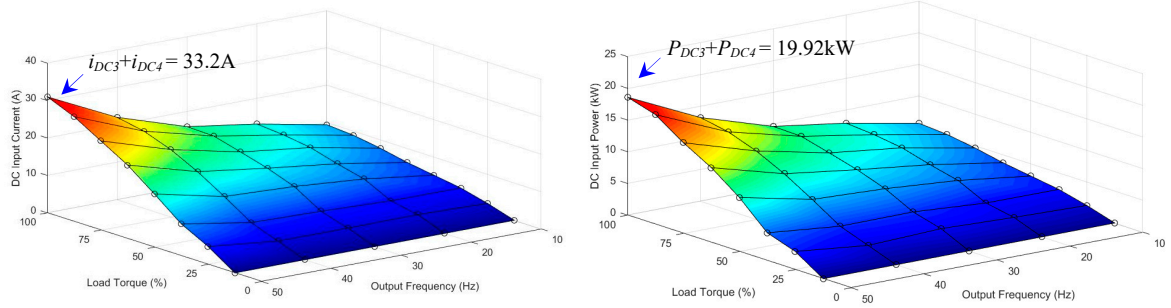

(**a**) (**b**)

Figure 26. The measured results of the three-phase dc-ac inverter for the air pump motors (i.e. modules 3 and 4) under variable load torque (25 – 100%) and output frequency (10 – 50Hz): (**a**) dc input current (i_{DC3}+i_{DC4}); (**b**) dc input power (P_{DC3}+P_{DC4}).

4.2.3. The dc-ac Inverter for 220VAC single-phase power supply (inverter module 5)

The simulation and experiment of the dc-ac inverter for the 220 VAC single-phase power supply (inverter module 5) are undertaken under the following conditions: (a) the overhead contact line voltage (v_{DC}) is 600VDC; (b) the resistive load is varied between 0% (no load) and 100% (full load); and (c) the output frequency (f_s) is 50Hz.

The performance metrics of inverter module 5 include (i) the waveform of input voltage (i.e., overhead contact line voltage; v_{DC}); (ii) the waveform of input current of module 5 (i_{DC5}); (iii) the waveform of output voltage (v_{5s}); (iv) the waveform of output current (i_{5s}); and (v) the input power of module 5 (P_{DC5}) by multiplying v_{DC} by i_{DC5}.

Preprints (www.preprints.org) | NOT PEER-REVIEWED | Posted: 1 May 2023 doi:10.20944/preprints202305.0020.v1

Figure 27 (a) and (b) respectively show the simulated and measured v_{DC}, i_{DC5}, v_{5s} and i_{5s} waveforms of the dc-ac inverter for the single-phase power supply (module 5) under the full load condition (resistive load = 100%), given v_{DC} = 600V and f_s= 50Hz. The corresponding v_{DC}, i_{DC5}, v_{5s} and i_{5s} waveforms of module 5 under no load condition (resistive load = 0%) are illustrated in Figures 27 (c) and (d).

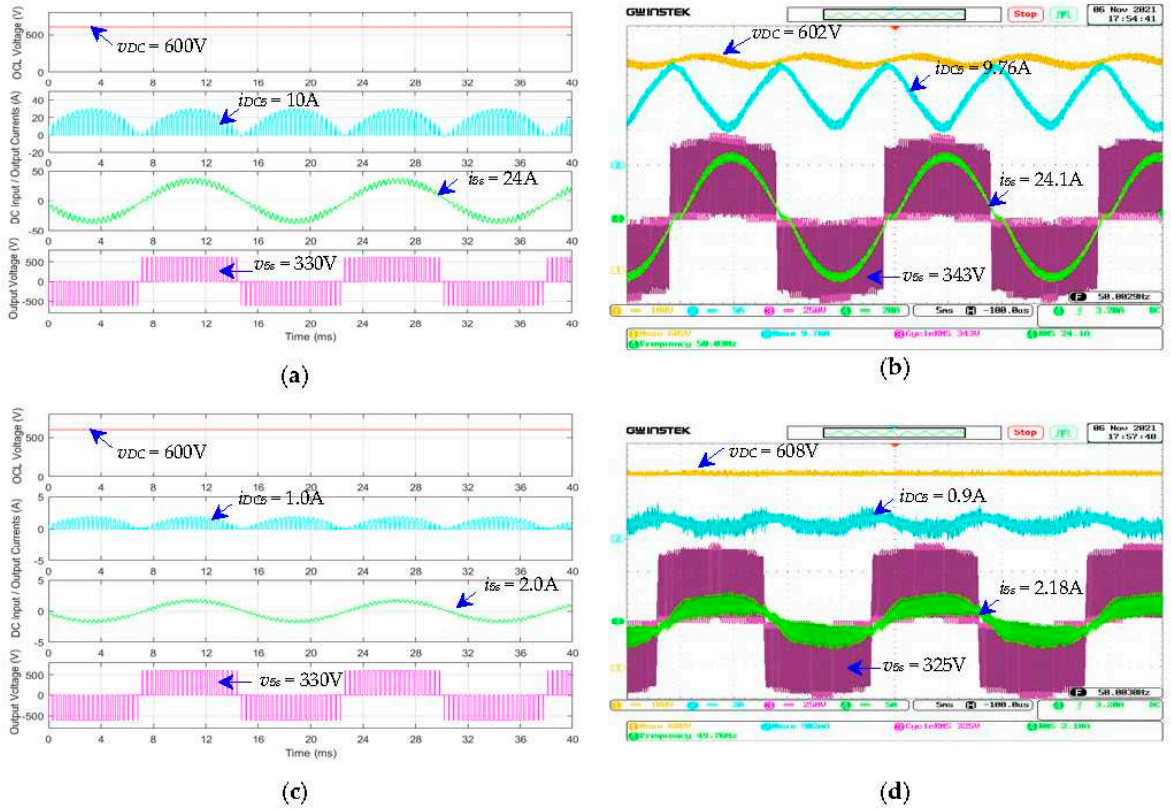

Figure 27. The v_{DC}, i_{DC5}, v_{5s}, and i_{5s} waveforms of the dc-ac inverter for the single-phase power supply (module 5) given v_{DC}= 600VDC and f_s= 50Hz: (**a**) full load (simulated; resistive load = 100%); (**b**) full load (measured); (**c**) no load (simulated; resistive load = 0%); (**d**) no load (measured).

Under the full load condition (Figure 27 (a)-(b)), the simulated and measured v_{DC}, i_{DC5}, v_{5s}, and i_{5s} are 600V and 602V; 10A and 9.76A; 330V and 329V; and 24A and 24.10A. The simulated and measured input power (P_{DC5}) of the dc-ac inverter for the 220VAC single-phase power supply at full load are 6.0 kW and 5.87kW. Meanwhile, under no load condition (Figure 27 (c)-(d)), the simulated and measured v_{DC}, i_{DC5}, v_{5s}, and i_{5s} are 600V and 608V; 1.0A and 0.9A; 330V and 325V; and 2.0A and 2.18A. The simulated and measured input power (P_{DC5}) of the dc-ac inverter for the 220VAC single-phase power supply at full load are 0.6 kW and 0.58kW.

4.2.4. Maximum input power consumption of auxiliary power supply system

The total input power consumption (P_{DCT}) of the proposed APS system are the summation of the input power of inverter modules 1 – 5 (P_{DC1}, P_{DC2}, P_{DC3}, P_{DC4}, P_{DC5}) under full load condition. Table 2 tabulates the simulated and measured maximum input current (i_{DC}) and input power (P_{DC}) of the dc-ac inverters (modules 1 – 5) of the proposed APS system under full load condition.

Table 2. The simulated and measured maximum input current and input power of the dc-ac inverters (modules 1 – 5) of the APS system under full load condition, given the overhead contact line voltage (v_{DC}) of 600V.

Onboard Electric Loads	Details	Measured	Simulated	% Error
Compressor motors	i_{DC1}	37.9A	37A	2.37
(2 units; modules 1 and2)	P_{DC1}	22.74kW	22kW	3.25

Preprints (www.preprints.org) | NOT PEER-REVIEWED | Posted: 1 May 2023 doi:10.20944/preprints202305.0020.v1

	i_{DC2}	37.9A	37A	2.37
	P_{DC2}	22.7kW	22kW	3.25
Air pump motors	i_{DC3}	16.6A	16A	3.61
(2 units; modules 3 and 4)	P_{DC3}	9.96kW	9.6kW	3.61
	i_{DC4}	16.6A	16A	3.61
	P_{DC4}	9.96kW	9.6kW	3.61
Resistive load	i_{DC5}	9.76A	10A	2.45
(Module 5)	P_{DC5}	5.85kW	6.0kW	2.56

Figure 28 shows the measured total input current of modules 1 – 4 (i_{DC1}+i_{DC2}+i_{DC3} +i_{DC4}) under variable load torque (25 – 100%) and output frequency (10 – 50Hz), given the overhead contact line voltage (v_{DC}) of 600V. The measured total input current of the dc-ac inverters for the compressor motors and air pump motors (modules 1 – 4; i_{DC1} + i_{DC2}+ i_{DC3} + i_{DC4}) under full load condition (100% load torque and 50Hz) is 109A. Meanwhile, the corresponding simulated i_{DC1} + i_{DC2}+ i_{DC3} + i_{DC4} is 108A.

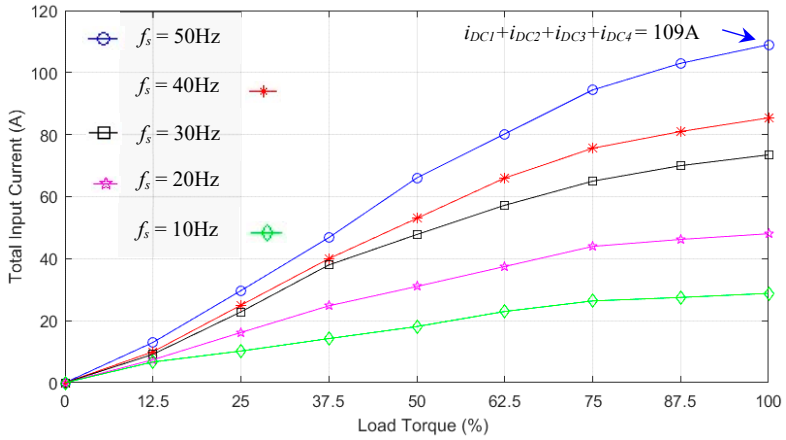

Figure 28. The measured total input current of the dc-ac inverters for compressor motors and air pump motors (modules 1 – 4; i_{DC1}-i_{DC4}) under variable load torque (25 – 100%) and output frequency (10 – 50Hz), given the overhead contact line voltage (v_{DC}) of 600V.

Figure 29 shows the measured total input power of modules 1 – 4 (P_{DC1} + P_{DC2} + P_{DC3} + P_{DC4}) under variable load torque (25 – 100%) and output frequency (10 – 50 Hz), given the overhead contact line voltage (v_{DC}) of 600V. The measured total input power of the dc-ac inverters for the compressor motors and air pump motors (modules 1 – 4; P_{DC1} + P_{DC2} + P_{DC3} + P_{DC4}) under full load condition is 65.4kW. Meanwhile, the corresponding simulated P_{DC1} + P_{DC2} + P_{DC3} + P_{DC4} is 64.8kW.

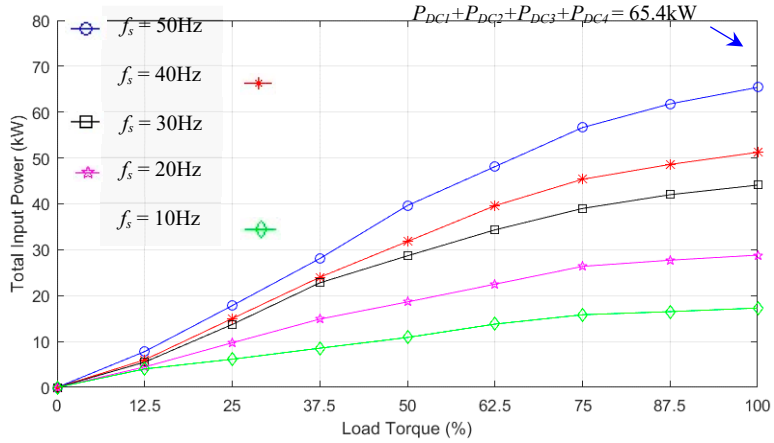

Preprints (www.preprints.org) | NOT PEER-REVIEWED | Posted: 1 May 2023 doi:10.20944/preprints202305.0020.v1

Figure 29. The measured total input power of the dc-ac inverters for compressor motors and air pump motors (modules 1 – 4; P_{DC1}-P_{DC4}) under variable load torque (25 – 100%) and output frequency (10 – 50Hz), given the overhead contact line voltage (v_{DC}) of 600V.

Figure 30 shows the measured total input current of modules 1 – 5 (i_{DCT}) under variable load torque (25 – 100%) and output frequency (10 – 50Hz), given the overhead contact line voltage (v_{DC}) of 600V. The measured total input current of modules 1 – 5 (i_{DCT}) under full load condition is 118.76A. Meanwhile, the corresponding simulated i_{DCT} is 120A.

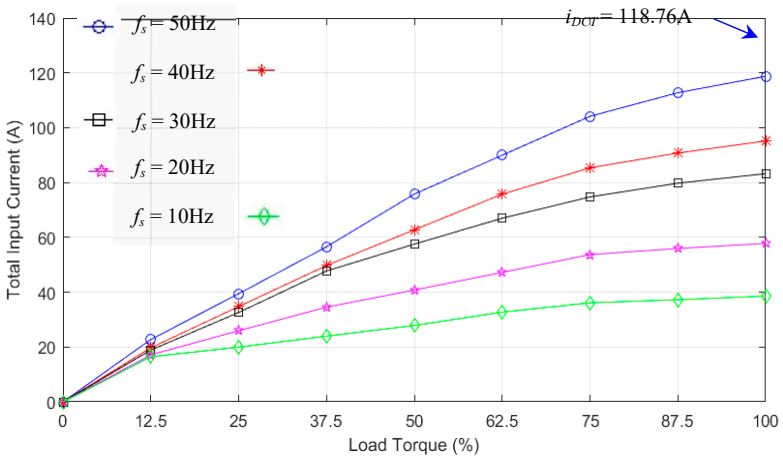

Figure 30. The measured total input current of the dc-ac inverters modules 1 – 5 (i_{DCT}) under variable load torque (25 – 100%) and output frequency (10 – 50Hz) for modules 1 – 4 and resistive load of 100% and output frequency of 50Hz for module 5, given the overhead contact line voltage (v_{DC}) of 600V.

Figure 31 shows the measured total input power of modules 1 – 5 (P_{DCT}) under variable load torque (25 – 100%) and output frequency (10 – 50Hz), given the overhead contact line voltage (v_{DC}) of 600V. The measured total input power of modules 1 – 5 (P_{DCT}) under full load condition is 71.25kW. Meanwhile, the corresponding simulated P_{DCT} is 70kW.

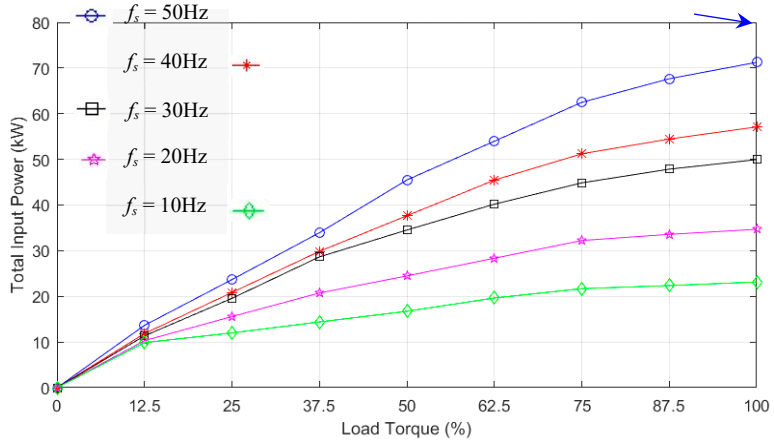

Figure 31. The measured total input power of the dc-ac inverters modules 1 – 5 (P_{DCT}) under variable load torque (25 – 100%) and output frequency (10 – 50Hz) for modules 1 – 4 and resistive load of 100% and output frequency of 50Hz for module 5, given the overhead contact line voltage (v_{DC}) of 600V.

Figure 32 depicts the 600VDC low-floor light rail vehicle (LRV) with the roof-mounted APS system. The LRV is to be officially launched and in service by June 2023 in Thailand's northeastern province of *Khon Kaen* (i.e., a second-tier city), located 450 km northeast of the capital Bangkok.

Preprints (www.preprints.org) | NOT PEER-REVIEWED | Posted: 1 May 2023 doi:10.20944/preprints202305.0020.v1

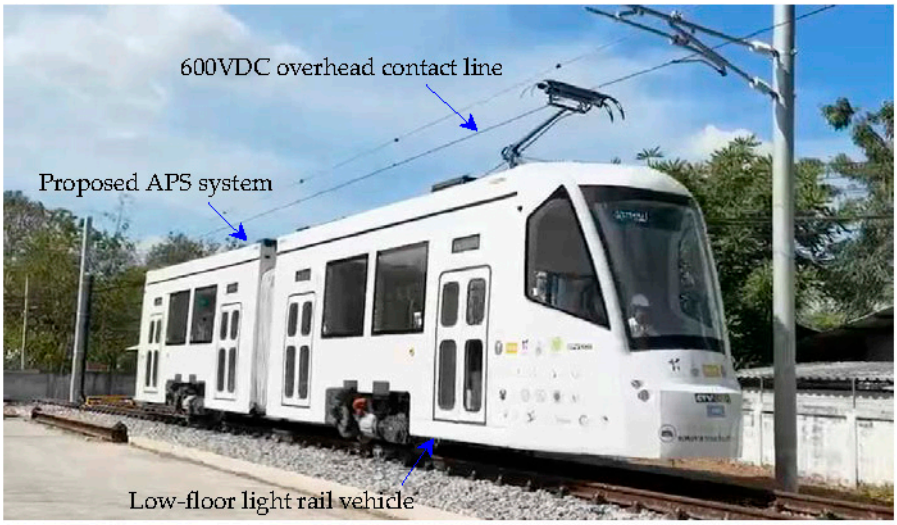

Figure 32. Low-floor light rail vehicle with the roof-mounted APS system.

5. Conclusion

This research proposed a roof-mounted APS system for 600VDC low-floor LRV, consisting of five parallel-connected inverter modules (modules 1 – 5). The inverter modules 1 and 2 are three-phase dc-ac inverters for compressor motors of the cooling system, and modules 3 and 4 are three-phase dc-ac inverters for air pump motors of the braking system. The inverter module 5 is single-phase dc-ac inverter for 220VAC power supply for onboard electric loads, including lighting, fans, CCTV cameras, electric doors, and 24VDC battery charging system. The v/f control method is used to vary the speed of the three-phase compressor motors of the cooling system (modules 1 and 2) and the three-phase air pump motors of the braking system (modules 3 and 4) of the low-floor LRV. The magnitude control is applied to module 5 for 220VAC output voltage and 50Hz output frequency. Simulations and experiments were carried out under variable load torque (25 – 100%) and output frequency (10 – 50Hz) for modules 1 – 4; and under full resistive load and no resistive load for the inverter module 5. The measured total input current (i_{DCT}) and total input power (P_{DCT}) of the proposed APS system under full load condition are 118.76A and 71.25kW, respectively. The experimental results indicate that the proposed APS system is operationally applicable to the 600VDC low-floor RLV. Subsequent research deals with the design and development of the roof-mounted traction system of the 600VDC low-floor LRV and the traction substation.

Author Contributions: Conceptualization, P.K. and K.C.; methodology, P.K., K.C., and S.K.; software, P.K.; validation, P.K., K.C. and S.K.; formal analysis, P.K.; investigation, K.C.; resources, S.K.; data curation, P.K.; writing—original draft preparation, P.K., K.C. and S.K.; writing—review and editing, P.K., K.C. and S.K.; visualization, P.K., K.C. and S.K.; project administration, P.K., K.C. and S.K.; funding acquisition, P.K., K.C. All authors have read and agreed to the published version of the manuscript.

Funding: This research was funded by the Program Management Unit for Competitiveness (PMUC), the Office of National Higher Education Science Research and Innovation Policy Council, Ministry of Higher Education, Science, Research and Innovation, Thailand, under grants no. C10F630062, C10F640250, and C10F650144.

Data Availability Statement: The data presented in this study are available on request from the corresponding author.

Conflicts of Interest: The authors declare no conflict of interest.

References

1. Fang, Y.; Jiang, Y.; Fei, W. Disruption recovery for urban public tram system: An analysis of replacement service selection. *IEEE Access* **2020**, 8, 31633-31646. [CrossRef]
2. Guerrieri, M. Tramways in urban areas: An overview on safety at road intersections. *Urban Rail Transit* **2018**, 4, 223-233. [CrossRef]
3. Mora, J. A streetcar named light rail. *IEEE Spectrum* **1991**, 28, 54-56. [CrossRef]
4. Swanson, J.D.; Thornes, C. Light-rail transit systems. *IEEE Vehicular Technology Magazine* **2010**, 5, 22-27. [CrossRef]
5. Glickenstein, H. Extension of the Hudson Bergen light rail. *IEEE Vehicular Technology Magazine* **2006**, 1, 40-43. [CrossRef]
6. Chan, H.Y.; Chen, A.; Li, G.; Xu, X.; Lam, W. Evaluating the value of new metro lines using route diversity measures: The case of Hong Kong's mass transit railway system. *Journal of Transport Geography* **2021**, 91, 1-16. [CrossRef]
7. Gunduz, M.; Ugur, L.O.; Ozturk, E. Parametric cost estimation system for light rail transit and metro trackworks. *Expert Systems with Application* **2011**, 38, 2873-2877. [CrossRef]
8. Song, H.; Schnieder, E. Development and validation of a distance measurement system in metro lines. *IEEE Transactions on Intelligent Transportation Systems* **2018**, 20, 441-456. [CrossRef]
9. Yang, X.; Ning, B.; Li, X.; Tang, T. A two-objective timetable optimization model in subway systems. *IEEE Transactions on Intelligent Transportation Systems* **2014**, 15, 1913-1921. [CrossRef]
10. Hoshi, M.; Murakami, N.; Ookubo, Y.; Arai, T.; Kono, H.; Aruga, H. Development of bogie for user friendly, extra low floor, light rail vehicle (LRV) using independent wheel system and next generation LRV. *Mitsubishi Heavy Industries, Ltd. Technical Review* **2007**, 44, 1-4 [CrossRef]
11. Lin, Y.C.; Lin, C.L.; Shieh, N.C. A hybrid evolutionary approach for robust active suspension design of light rail vehicles. *IEEE Transactions on Control Systems Technology* **2006**, 14, 695-706. [CrossRef]
12. Matsuoka, K. Development trend of the permanent magnet synchronous motor for railway traction. *IEEJ Transactions on Electrical and Electronics Engineering* **2007**, 2, 154-161. [CrossRef]
13. Mizuno, S.; Noda, S.; Matsushita, M.; Koyama, T.; Shiraishi, S. Development of a totally enclosed fan-cooled traction motor. *IEEE Transactions on Industry Applications* **2013**, 49, 1508-1514. [CrossRef]
14. Youssef M.Z.; Woronowicz, K.; Aditya, K.; Azeez, N.A.; Williamson, S.S. Design and development of an efficient multilevel dc/ac traction inverter for railway transportation electrification. *IEEE Transactions on Power Electronics* **2016**, 31, 3036-3042. [CrossRef]
15. Lin, Y.C.; Lin, C.L.; Yang, C.C. Robust active vibration control for rail vehicle pantograph. *IEEE Transactions on Vehicular Technology* **2007**, 56, 1994-2004. [CrossRef]
16. Li, K.; Cheng, S.; Yu, T.; Wu, X.; Xiang, C.; Bilal, A. An on-line multiple open-circuit fault diagnostic technique for railways vehicle air-conditioning inverters. *IEEE Transactions on Vehicular Technology* **2020**, 69, 7026-7039. [CrossRef]
17. Dolgushin, A.S.; Ganshin, A.A.; Meleshin, V.I.; Zhiklenkov, D.V. Auxiliary large power converter supplying with 2.1…4.7kV DC contact line for Russian railways. In Proceedings of the 20th European Conference on Power Electronics and Applications (EPE'18 ECCE Europe), Riga, Latvia, 17-21 Sep. 2018.
18. Rufer, A.; Schibli, N.; Chabert, C.; Zimmermann, C. Configurable front-end converter for multicurrent locomotives operated on 16 2/3Hz AC and 3kV DC systems. *IEEE Transactions on Power Electronics* **2003**, 18, 1186-1193. [CrossRef]
19. Vinnikov, D.; Laugis, J.; Jalakas, T. Development of auxiliary power supplied for the 3.0kV DC rolling stock. In Proceedings of 2007 IEEE International Symposium on Industrial Electronics, Vigo, Spain, 4-7 Jun. 2007.
20. Deblecker, O.; Moretti, O.; vallee, F. Comparative study of soft-switched isolated dc-dc converter for auxiliary railway supply. *IEEE Transactions on Power Electronics* **2008**, 23, 2218-2229. [CrossRef]
21. Vinniskov, D.; Laugis, J. High voltage auxiliary power supply with the simplified power circuit topology for the DC trains. In Proceedings of the 9th International Conference on Electrical Power Quality and Utilization, Barcelona, Spain, 9-11 Oct. 2007.
22. Vos, P.G.E. The auxiliary power supply system for double deck trains. In Proceedings of the IEEE Colloquium on Auxiliary Power Supplied for Rolling Stock, London, UK, 24 Feb. 1992.
23. Baars, N.H.; Everts, J.; Huisman, H.; Duarte, J.L.; Lomonova, E.A. A 80-kW isolated dc-dc converter for railway applications. *IEEE Transactions on Power Electronics* **2015**, 30, 6639-6647. [CrossRef]

24. Mishima, T.; Koji, Y. Zero voltage soft-switching phase-shift PWM controlled three-level dc-dc converter for railway auxiliary electric power unit. In Proceedings of the IEEE Applied Power Electronics Conference and Exposition (APEC), Anaheim, CA, USA, 17-21 Mar. 2019. [CrossRef]
25. Ocklenburg, M.; Dohmen, M.; Wu, X.; Helsper, M. Next generation dc-dc converters for auxiliary power supplied with SiC MOSFETs. In Proceeding of the 2018 IEEE International Conference on Electrical Systems for Aircraft, Railway, Ship Propulsion and Road Vehicles & International Transportation Electrification Conference (ESARS-ITEC), Nottingham, UK, 7-9 Nov. 2018.
26. Helsper, M.; Ocklenburg, M.A. SiC MOSFET based auxiliary power supplied for railway vehicles. In Proceedings of the 20th European Conference on Power Electronics and Applications (EPE'18 ECCE Europe), Riga, Latvia, 17-21 Sep. 2018.
27. Ocklenburg, M.A.; Helper, M.; Siemer, H.; Gusek, A. Potentials and requirements of silicon carbide hybrid power modules for railway onboard auxiliary power supplied. In Proceedings of the International Exhibition and Conference for Power Electronics, Intelligent Motion, Renewable Energy and Energy Management (PCIM Europe 2014), Nuremberg, Germany, 20-22 May 2014.
28. Marz, A.; Bakran, M.M. Designing a low weight low loss auxiliary converter for railway application. In Proceedings of the International Exhibition and Conference for Power Electronics, Intelligent Motion, Renewable Energy and Energy Management (PCIM Europe 2014), Nuremberg, Germany, 20-22 May 2014.
29. Cobanov, N.; Tezak, N. Soft-switching converter for tram auxiliary power supply. In Proceedings of the 16th International Power Electronics and Motion Control Conference and Exposition, Antalya, Turkey, 21-24 Sep. 2014.
30. Martinez, C.; Vazquez, R.; Quesada, I.; Lucena, C.; Lazaro, A.; Barrado, A. PWM-VSI overmodulation technique with carrier harmonics reduction for auxiliary railway power supply. In Proceedings of the 7th International Conference-Workshop Compatibility and Power Electronics (CPE), Tallinn, Estonia, 1-3 June 2011.
31. Nguyen, P.; Gerth, A. Softswitching with SiC-devices for compact onboard railway power supplies. In Proceedings of the 15th International Power Electronics and Motion Control Conference (EPE-PEMC 2012 ECCE Europe), Novi Sad, Serbia, 4-6 Sep. 2012.
32. Pons, E.; Tommasini, R.; Colella, P. Fault current detection and dangerous voltage in DC urban rail traction systems. *IEEE Transactions on Industry Applications* **2017**, 53, 4109-4115.